Model of potential drill target and proposed drill path

Deliverable D8.1

Model of potential drill target and proposed drill path

Deliverable D8.1

Editor: Franceso Parisio

Responsible WP-leader: Ernst Huengers

Work package 8, Task 8.1

May 2020

Website: http://www.gemex-h2020.eu

The GEMex project is supported by the European Union's Horizon 2020 programme for Research and Innovation under grant agreement No 727550 and the Mexican Energy Sustainability Fund CONACYT-SENER, project 2015-04-268074

Table of Contents[1]

[1] The content of this report reflects only the authors' view. The Innovation and Networks Executive Agency (INEA) is not responsible for any use that may be made of the information it contains.

Partner

Helmholtz Centre for Environmental Research (UFZ)

Francesco Parisio

Nederlandse Organisatie voor Toegepast Natuurwetenschappelijk Onderzoek (TNO)

Peter Fokker

Istituto Nazionale di Oceanografia e di Geofisica Sperimentale (OGS)

Biancamaria Farina, Flavio Poletto

Helmholtz Centre Potsdam – German Research Centre for Geosciences (GFZ)

Katrin Kieling, Ernst Huenges

Fraunhofer-Einrichtung für Energieinfrastrukturen und Geothermie (IEG)

Michal Kruszewski

Consiglia Nazionale Delle Ricerche (CNR)

Giordano Montegrossi

Rheinisch-Westfälische Technische Hochschule Aachen (RWTH)

Paromita Deb, Xiangyun Shi

Executive summary

This report is Deliverable 8.1 “Model of the potential drill target and proposed drill path” of the Horizon2020 GEMex project (GA No. 727550).

The Los Humeros geothermal reservoir is home of one of the largest geothermal power plants in Mexico, with an installed capacity of around 95 MWe. The current power plant includes some 60 wellbores drilled up to approximately 3 km depth and with maximum temperature of around 380 °C. Future development plans include deepening the reservoir beyond the current production zones and reaching for supercritical fluids. Drilling a wellbore in such an environment is a complex task and locating targets and possible scenarios has to rely on predictive models. This deliverable summarizes the physics-based models that have been developed during GEMex to forecast the complex interaction between deep wells and the surrounding rocks. Models are based on latest findings on the state of stress at the Los Humeros caldera and include thermal diffusion models, models for the brittle-ductile transition depth, seismic models of wave propagation and wellbore stability models. We show that, despite the vast uncertainties that are typical of such ambitious goals, the proposed models can be valuable tools helping to successfully drill in the Los Humeros field the first supercritical geothermal wellbore in Latin America.

1 Introduction

The Los Humeros geothermal field (LHGF) is located at the eastern section of the Trans-Mexican Volcanic Belt (TMVB) and is one of the four most productive geothermal fields in Mexico. It consists of approximately 25 production and several injection wells with a total installed power of approximately 95 MWe (Norini et al., 2019). The eastern section of the TMVB is defined by the ENE-WSW trending principal stress direction and a normal faulting stress regime (Suter 1991). The present geological configuration of the field results from the complex interplay between the regional stress field, and the eruptive activity within the Los Humeros caldera.

Three main fault systems control the ascent of fluids within the caldera: i) the first one is the NW-SE trending system in the south of the field and shifts towards the NNW-SSE and N-S direction; ii) the second one is the E-W trending system in the eastern side of the caldera, where it is cut by iii) multiple secondary oblique WNW-striking structures (Carrasco-Núñez et al., 2015). The most prolific producing wells are located in the northern part of the system, where hot fluid circulates mainly through the active NNW-SSE east-dipping structures. To compensate reservoir depletion, water is re-injected in the northern part of the reservoir. Non-productive wells are located in the vicinity of the E-W trending systems in the eastern part of the geothermal field and the region west from the NNW-SSE striking faults (Norini et al., 2015 and 2019). The fluids within the Alseseca, Teziutlan and Cuyuaco andesites are sealed upwards by the low permeability Quaternary ignimbrites, which act as cap rocks. A low permeability basement composed of Cretaceous-Jurassic limestones underlines the fractured reservoir. The basement carbonate has partially metamorphosed to marbles and skarns by granitic intrusions (Norini et al., 2015).

Since the late 1970s, extensive exploration expeditions within the Los Humeros caldera aimed at electricity generation provided a plethora of information. All 60 wellbores were drilled up to approximately 3000 m depth. This contribution discusses the potential drilling of a deeper wellbore which aims at reaching supercritical fluid conditions. Drilling into a supercritical reservoir and accommodating long-term, sustainable and safe production from such a resource is a highly complex task that is filled with uncertainty and, although several scenarios can be envisioned, unexpected outcomes are always possible. As an example, the successful drilling of the IDDP-2 well in Iceland that reached supercritical fluids at 4.5 km depth was preceded by two failed attempts in the previous decade (Friðleifsson et al., 2018).

The final target of a deep wellbore is highly influenced by the available financial resources, the overall objectives and the risks of failure that operators are willing to take. Drilling a wellbore in high-temperature environments entails some specific issues related to the behaviour of rocks, fluids, wellbore construction and drilling equipment at high temperatures. Conventionally used well completion materials, drilling fluids, downhole drilling tools, borehole logging and monitoring equipment are not designed to withstand temperatures in excess of 374°C (i.e., critical temperature of pure water), which can lead to critical wellbore failures and, as a result, to the total well abandonment. Additionally, interaction of drilling equipment and/or wellbore construction with hostile reservoir fluids enables processes such as corrosion and/or scaling (Kruszewski &

Wittig, 2018). Corrosion of metallic materials is one of the most pervasively occurring causes for premature failure of downhole components in geothermal wells. To optimise material selection, materials were investigated in task 8.2 of work package 8 in bypass/downhole installations in real geothermal environments in Los Humeros wells (Ingólfur Örn Þorbjörnsson 2019).

We have developed several methods and modelling approaches to address the scientific and technical issues that serve as a basis for future drilling into a supercritical reservoir. The deliverable firstly introduces what is known about the state of stress at Los Humeros and discusses the results of thermal modelling. A model for the brittle-ductile transition depth provides estimates of the potential overlap between the brittle-fractured crust and supercritical fluids. A model for seismic attenuation at high temperature can be used to forecast the presence of melting during drilling. A semi-analytical solution for wellbore failure at high temperature concludes the list of methods. A final discussion provides the current status and potential outlook for developing supercritical resources at the Los Humeros geothermal field.

2 State of stress

The in-situ stress tensor is one of the primary controls on wellbore stability, reservoir depletion, and stimulation performance in any type of geothermal reservoir. For example, a mode-I tensile fracture propagates perpendicular to the direction of the minimum principal stress and the orientation and magnitude of the maximum principal stress governs slip and opening of natural fractures and faults (Zoback 2007). Therefore, it is highly desirable for any type of drilling or stimulation operation to determine the orientation and magnitude of the in-situ stress field.

Direct in-situ stress measurements such as leak-off (LOT), over-coring tests, or hydrofracturing are in most cases not part of drilling operations in high-temperature geothermal fields. High temperature limits the usage of downhole equipment and increases substantially the cost of measurements. When no direct in-situ measurement is available, the state of stress can be evaluated with indirect information such as, e.g., geological observations (i.e., fault slip observations, volcanic vent alignments, and petal centreline fractures), borehole deformations (i.e., drilling-induced fractures, DIF's, and borehole breakouts, BO's) and focal earthquake mechanisms (Heidbach et al., 2016).

Figure 1 shows a summary of the stress indicators observed within the Los Humeros caldera.

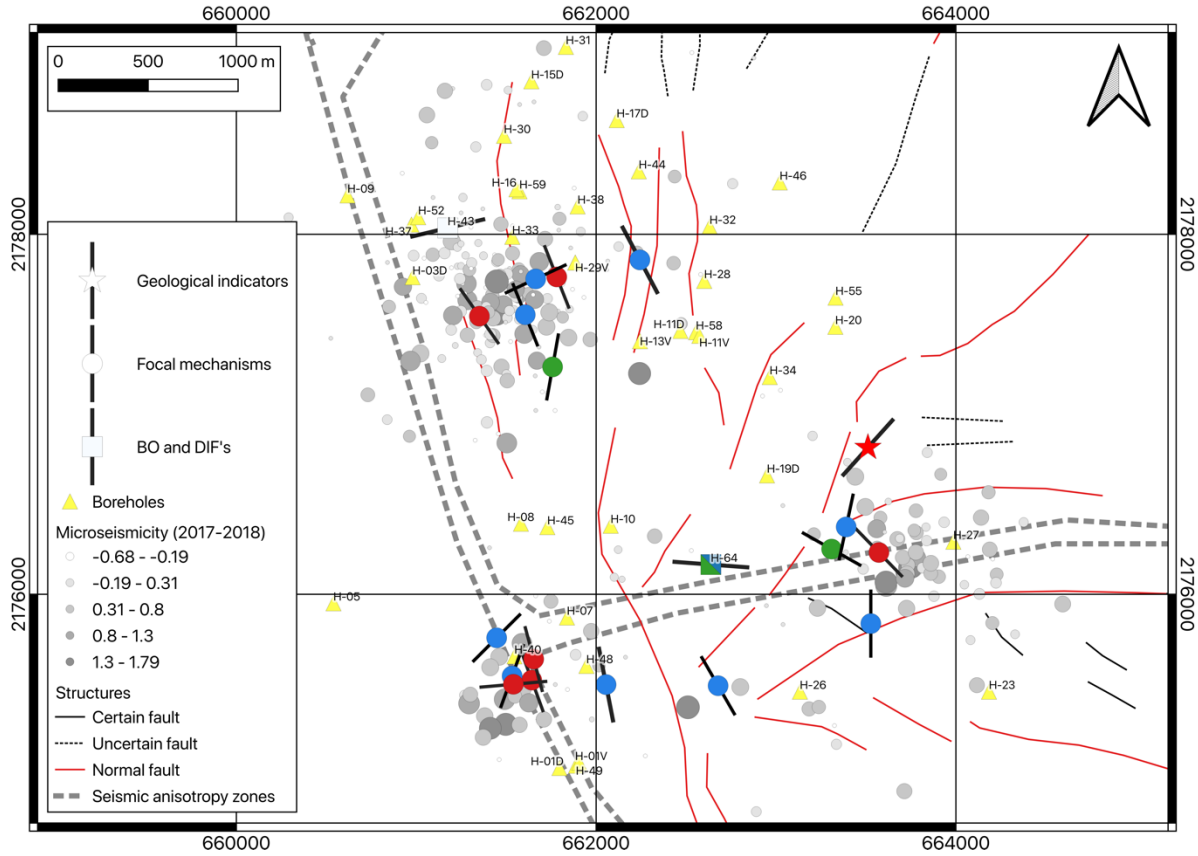

Figure 1: The stress map of LHGF with stress indicators based on studies by Kruszewski et al., (2020 submitted), Heidbach et al. (2016), Lermo et al. (2016), Lorenzo-Pulido (2008), Jousset et al. (2019), and Toledo et al. (2019); blue marker color indicates reverse faulting, green – strike-slip, red – normal faulting, and white – unknown; microseismicity data recorded between 2017 and 2018 by Toledo et al. (2019); seismic anisotropy zones from Rodriguez et al. (2012); location of faults from Lepillier et al. (2020) (Kruszewski et al., 2020 submitted).

A single type C quality measurement from the World Stress Map (WSM) dataset is available within the Los Humeros caldera (Heidbach et al., 2016). The volcanic vent alignment observation is located in the central-eastern section of the geothermal field and indicates an SHmax azimuth of 42 ±8º NE with a normal faulting regime. Formation Micro Imaging (FMI) log from well H-43 located in the north-western part of the field showed 11 drilling-induced fractures (DIF) between 1250 and 1633 m depth and 3 DIF's between 1711 and 1813 m (Lorenzo-Pulido 2008). All observed pre-existing fractures from the FMI log have a constant N-S to NNE-SSW strike and align with the direction of the observed normal faults in the northern part of the field (Norini et al., 2019). Between 1250 and 1633 m, DIF's strike in NNE-SSW and ENE-WSW direction that is parallel to surface traces of faults (i.e., normal faulting regime). Between 1711 and 1813 m depth, DIF's strike in the WNW-ESE direction, which is perpendicular to the observed faults in the field and agrees with a compressive stress regime (Norini et al., 2019). The change of direction of DIF's from H-43 well indicates a 90º rotation of the direction of SHmax in the deeper section of the LHGF reservoir.

A magnitude 2.0 earthquake at a depth of 1600 m and a magnitude 4.2 one at depth of 1900 m struck on the 16/08/2015 and 08/02/2016, respectively: focal plane inversion indicated a reverse faulting regime with maximum stress striking in the NNW-SSE direction for both events, which epicenters are located along the trace of the Maxtaloya-Los Humeros fault (Lermo et al., 2016). This observation agrees with the DIF's located at the deeper sections of the H-43 well and has relatively similar direction to the mapped faults located in the vicinity of the two epicentres.

Focal mechanism analysis of 17 events recorded between 2017 and 2018 indicates a stress regime oscillating between normal and reverse faulting with major stress direction from NW-SE to NE-SW (Jousset et al., 2019). Events magnitudes range from -0.68 and 2.21 at a depth between 2000 and 3700 m. The majority of the focal mechanisms registered in the northern part of the field follow the NNW-SSE direction, whereas events in the southern part present no visible stress trends. Strong variations of the in-situ stress regime with depth were observed (Jousset et al., 2019; Toledo et al., 2019).

Further analyses on microseismic activity between 2017 and 2018 evidenced that all earthquakes are localised in three major clusters located in the i) north-western, ii) central-eastern and iii) central-western area of the geothermal field (Jousset et al., 2019; Toledo et al., 2019). Spatial distribution agrees with previous observations (Lermo et al., 2007 and 2008; Gutierrez-Negrin et al., 2004) of higher frequency of seismic events where geothermal operations of fluid injection and production occur (i.e., wells H-29 and H-38). The second largest cluster in terms of number of recorded events is located in the vicinity of the H-40 and H-7 wells, while the third one is located west from the H-27 well. Most events are located between 1 and 3 km depth, with a peak of frequency corresponding to the depth of the current production zone of 2.5 km.

Observations of seismic anisotropy based on events recorded between 1997 and 2008 suggest that 3 zones of similar major stress directions are present within the geothermal field (Rodriguez et al., 2012). Zone A is located in the central part of the field (i.e., east from the Los Humeros fault), follows a NE-SW direction (approximately 30º NE) parallel to the regional stress. The stress

direction in this area agrees with the observation of major stress azimuth from the volcanic vent alignments and borehole observations from the H-43 well. Zone B is located in the most southern and most northern parts of the geothermal field, where major stress has an E-W trend (approximately 85º E). Zone C is located in the western part of the field (i.e., west from the Los Humeros fault) and major stress follows a NW-SW direction (approximately 45 NWº) in agreement with observations from earthquake focal mechanisms registered close to the Los Humeros and Maxtaloya faults.

Overall, the local in-situ stress state within the Los Humeros geothermal field is strongly heterogeneous and changes considerably between extensional and compressional stress regimes at different sections of the caldera and with depth. It is believed that the complex local stress field of the LHGF is related to the shallow magmatic or hydrothermal system of the caldera complex (Norini et al., 2019). Based on the analysis of the borehole deformations and information of circulation losses observed during drilling of the H-64 well, located in the central section of the geothermal field, potential strike-slip to reverse faulting stress regime was indicated (Figure 2) (Kruszewski et al., 2020 submitted).

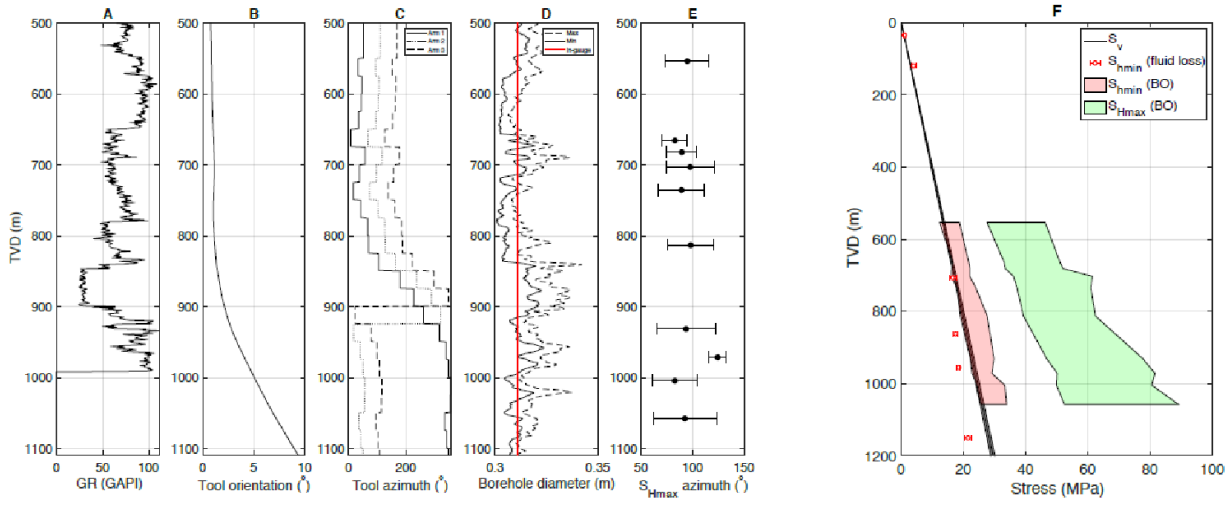

Figure 2: Results of the borehole breakout (BO) and in-situ stress tensor analysis from the H-64 well; A) gamma-ray (GR) log; B) six-arm caliper tool orientation; C) azimuth of caliper arms; D) semi-minor and -major borehole diameters with in-gauge diameter as a red line; E) azimuth of SHmax; F) in-situ stress tensor of the LHGF (shaded areas represent uncertainties) (Kruszewski et al., 2020 submitted).

3 Thermal model of Los Humeros

3.1 Temperature data from wells

Reliable thermal models are essential to plan and manage the exploitation of geothermal resources. To estimate the amount of extractable energy from a geothermal reservoir, it is necessary to know the vertical temperature distribution in the formations with considerable accuracy. The only direct measurements of subsurface temperature can be obtained from measurements performed in boreholes. The protocol for collecting temperature and pressure measurements varies depending on the operating company, but the usual practice is to run temperature logs with an interval of several hours immediately after drilling, followed by heating-up surveys conducted after a few weeks or months of shutting the well. The transient measurements immediately after drilling are useful guides for decision making regarding casing depths and completion of wells, but they are affected due to a number of factors such as drilling fluid, well design and permeability of the reservoir. Therefore, the most trustworthy measurements are usually obtained from heating-up surveys during which wells have sufficient time to regain their natural conditions.

In each well in the Los Humeros field, the transient temperature and pressure were recorded immediately after drilling and additional heating-up surveys in most wells were performed after shutting a well for several weeks or sometimes months. Regional hydrological studies and production information from wells indicated that the fluid flow in Los Humeros is controlled by faults and fractures (Cedillo-Rodríguez 2000; Arellano et al., 2003). Analysis of temperature and pressure data from the wells of Los Humeros (Deb et al., 2019c) indicate presence of multiple feeding zones in wells related to regional faults and fractures in the host rocks (Figure 3). The feeding zones contribute to flow within the wells, but mask the real temperature of the formation as the well cannot attain equilibrium with the formation due to the interzonal flow effects (Grant et al, 1983).

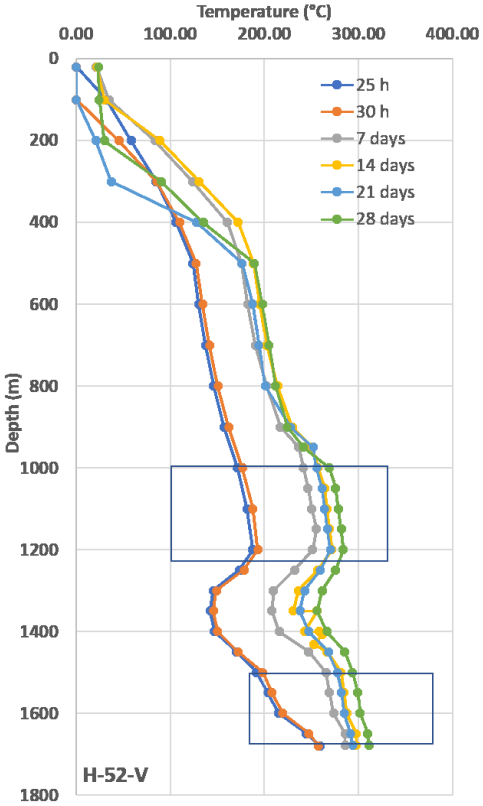

Figure 3: Transient temperature data of well H 52 showing the feeding zones.

To understand the natural steady-state conditions of Los Humeros geothermal system before production began, we performed 3D numerical simulation of heat transport and fluid flow. For calibration of our initial steady-state model, we corrected the transient temperature data to estimate pseudo-static conditions at the bottom-hole depth, away from the feeding zones. The bottom-hole depth is considered to be the least affected by drilling-induced thermal disturbance (Kutasov and Eppelbaum, 2005) and temperature data corresponding to this depth can be used to estimate static conditions using different methods. One of the most widely used methods is adapted from Horner (1951) due to the apparent similarity to the conventional pressure build up (Horner 1951; Dowdle and Cobb, 1975). Horner's method requires mud circulation times as inputs, which are not available for Los Humeros wells. Therefore, a reasonable circulation time of 6 hours was assumed for applying the correction to the bottom- hole data. The corrected BHT of different wells used for calibration are shown in Table 1.

Table 1: Bottom hole temperatures (BHT) of wells used for the calibration of the temperature model in Los Humeros.

Well	Coordinates		Elevation	Depth of correction	BHT
	UTM X	UTM Y	(masl)	(m)	(°C)
H-1-V	661906	2175064	2828	1408	274.19
H-2-V	662646	2172435	2896	2280	275
H-3-V	660622	2177903	2755	1650	315.69
H-5-V	660540	2175950	2762	1845	233
H-6-V	663508	2173545	2894	2540	323
H-7-V	661838	2175871	2782	2281	300
H-8-V	661582	2176392	2771	2300	394.03
H-9-V	660618	2178216	2752	2435	259
H-11-V	662574	2177436	2812	2376	356
H 13-V	662244	2177406	2835	2400	303
H-14-V	663832	2169627	2820	1373	126
H-15-V	661638	2178804	2795	1925	278
H-16-V	661557	2178250	2783	2038	339
H-17-V	662298	2178606	2813	2214	251
H-18-V	664916	2172077	3002	2885	297
H-19-V	662881	2176643	2808	2250	248
H-20-V	663330	2177486	2830	2389	345
H-21-V	662279	2179691	2871	2195	260
H-22-V	660055	2178853	2770	1539	271.67
H-23-V	664184	2175459	2872	2450	198
H-24-V	665497	2172938	2949	3263	259
H-25-V	666393	2176169	2800	2283	184
H-26-V	663133	2175459	2876	2440	326
H-28-V	662601	2177741	2820	2558	360
H-30-V	661488	2178547	2787	1902	234
H-31-V	661832	2179041	2810	1914	323
H-32-V	662631	2178043	2818	2186	332.13
H-33-V	661534	2177986	2782	1590	275
H-38-V	661897	2178155	2795	1390	169

3.2 Geological model

The geological model of Los Humeros is modeled in Work Package 3 (Calcagno et al., 2018) using well data and surface geological information and divides the regional stratigraphy into four broad units according to volcanological history. The four major groups represent the major events during

the evolution of the caldera system. These groups comprise the pre-volcanic basement comprising limestone and crystalline basement, the pre-caldera group, built by the andesite sections, the caldera group, mainly composed of ignimbrites and the post-caldera group, comprising different volcanic and alluvial deposits (Carrasco-Núñez et al., 2017; Norini et al., 2015). A smaller subset of this structural model is created with nine different geological units: basement, basal pre-caldera, intermediate pre-caldera, upper pre-caldera, Los Humeros caldera, intermediate caldera, Los Potreros caldera, post-caldera, and undefined pyroclastic rocks and 32 fault structures focusing on the area under exploitation by CFE. For modeling purposes, the basement is divided into two groups: sedimentary limestone and crystalline basement which results in 5 broad groups in regional model and 10 lithological units in the local reservoir model (Table 2, Figure 4). The structural models are parameterized using appropriate petrophysical properties obtained from laboratory measurements on representative outcrop samples and core data from Los Humeros (Table 3).

Table 2: Geological units of the reservoir model (WP3) [5]; Group IV is divided into two subgroups - limestone and granitic basement in the numerical model.

Groups	Units	Rock description	Age (Ma)
Group I: Post-caldera volcanism	U1: Undefined pyroclastic rocks	Tuff, pumice and some alluvium	< 0.003
	U2: Post caldera lava flow	Rhyodacites, andesites, basaltic andesites and olivine basalts lava flow	0.05 to 0.003
Group II: Caldera volcanism	U3: Los Potreros caldera	Rhyodacitic flows and Zaragoza Ignimbrites	0.069
	U4: Intermediate caldera	Faby Tuff and andesitic-dacitic lava flow	0.07
		Rhyolitic and obsidian domes	0.074
	U5: Los Humeos caldera	Mainly the Xaltipan Ignimbrite with minor andesitic and rhyolitic lavas	0.165
Group III: Pre-caldera volcanism	AP: Upper precaldera	Pyroxene andesites (Teziutlá Andesites) with mafic andesites in the basal part and/or dacites	2.61 to 1.46
	T: Pyroclastic rocks	Tuffs identified by CFE in most of the wells, between the andesitic rocks AH and AP	>2.61
	AH: Basal precaldera	Hornblende andesites (Alseseca Andesites and Cerro Grande) and dacites	10.5 to 8.9
Group IV: Limestone Basement	U9: Basement	Middle Miocene granitic intrusions	to
		Cretaceous limestones and shales and minor flint	~140
		Jurassic limestones and shales	~190
Group IV: Crystalline Basement	U10: Basement	Paleozoic granites and schists (Teziultán Massif)	>251

Table 3: Petrophysical properties of the geological units used for numerical modelling. Data from Deb et al. (2019a), Bär et al. (2019), Schön (2014), Rybach (1976), Rybach (1986).

Units	porosity [%]	permeability [m²]	matrix thermal conductivity [W/(m K)]	heat production rate [W/m³]	volumetric heat capacity [J/(m³K)]
U1: Undefined pyroclastic rocks	50.01	1.27E-14	1.91	5.00E-07	2016751
U2: Post caldera lava flow	12.80	1.18E-15	2.18	5.00E-07	2035034
U3: Los Potreros caldera	14.30	1.17E-17	2.74	1.48E-06	2117271
U4: Intermediate caldera	12.13	8.00E-16	2.31	1.50E-06	1992487
U5: Los Humeos caldera	14.30	1.17E-17	2.74	1.48E-06	2117271
AP: Upper precaldera	6.00	1.36E-16*	2.14	1.08E-06	2140839
T: Pyroclastic rocks	13.91	1.29E-15*	2.73	2.45E-06	1864517
AH: Basal precaldera	6.00	2.14E-16*	2.63	1.08E-06	2127233
U9: Basement	1.99	3.19E-18*	2.84	6.20E-07	2208692
U10: Basement	2.00	3.00E-18	3.20	2.45E-06	2208692
Faults	20.00	2.00E-15*	2.40	0.00E+00	2016751

Previous studies suggest the existence of two reservoir zones, the upper reservoir is composed of dominant liquid with hydrostatic pressure profile and neutral pH, while the lower one being steam dominated with steam static pressure profile and acidic fluid separated by low-permeability vitreous tuff (Cedillo-Rodríguez 2000). Other studies (Izquierdo et al., 2000) indicate that these are not two separate reservoirs but rather structurally controlled feeding zones originating from the same reservoir. In the WP 3 geological model, which is used for the current numerical modeling, the vitreous tuff layer is included as an impermeable layer separating the two andesitic reservoirs.

3.3 Numerical model

The numerical modeling is performed in two scales: regional and reservoir scale (Figure 4) focusing on the area under exploitation by CFE. The vertical extent of the regional model was reduced to 4.6 km below sea level and the model was discretised into cells of size 250 m × 250 m × 50 m resulting in a total of 6.2 million cells. The local model on the other hand was limited to 1 km below sea level, and was finely discretized in cubic cells of dimension of 50 m x 50 m x 50 m, also resulting in approximately 6.2 million cells.

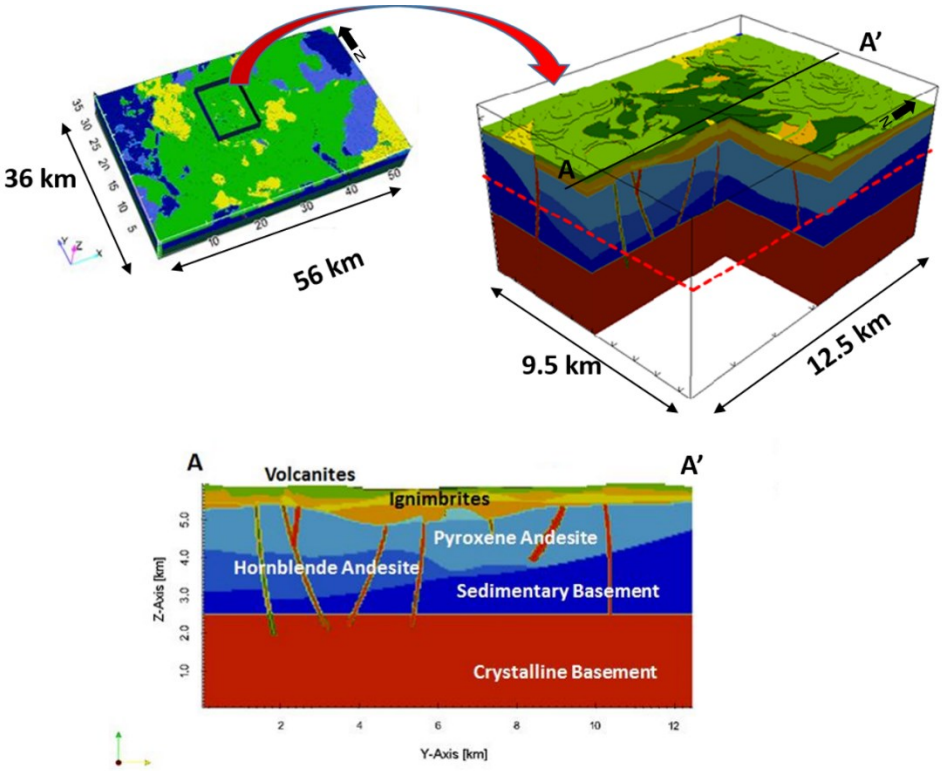

Figure 4: Geological model in regional (top left) and reservoir scale (top-right), the cross-section AA' shows the main reservoir rocks (andesites), the sealing ignimbrites and the overlying young volcanic rocks.

Numerical simulation is performed using the finite difference code SHEMAT-Suite (Clauser 2003; Rath et al., 2006), which solves the coupled steady-state or transient equations for groundwater flow, heat and reactive solute transport. Explanations on the governing equations are provided in Deb et al. (2019a) and Clauser (2003). The temperature boundary condition at the top of the model domain represented by the topographical surface is calculated using mean annual air temperature data obtained from Los Humeros climate station and topographic height. The pressure at the topographic surface is assumed to be atmospheric, implying the groundwater surface and therefore the hydraulic head coinciding with the topographic surface.

Initial conductive simulations were performed in regional scale to estimate the basal heat flow at a depth of 4.6 km below sea level. Wells H-25 and H-14 are the easternmost and southernmost wells of the caldera complex respectively, and are relatively colder than their western (H-5) and northern counterparts (H-21). Accordingly, several basal heat flow scenarios were assumed to understand the heterogeneity in temperature distribution observed in wells (Table 1). A regional specific heat flow of 91 mW m^{-2} is used for Zone 3 (Ziagos et al., 1985), while several simulation scenarios were investigated by varying the basal specific heat flow values under Los Humeros caldera (Zone 2) and Los Potreros caldera (Zone 1), (Figure 5). The results of the initial conductive simulations (Deb et al., 2019a; Deb et al., 2019b) suggested that the easternmost well of the Los Potreros caldera, H-25, and the southernmost well H-14, require a basal specific heat flow of the order of 225 mW m^{-2} – 250 mW m^{-2} for an acceptable match with the well data while the temperatures observed in wells H-5, H-21 and H-22 required much higher heat flux values (> 350

mW m^{-2}) to explain the observed temperature. Therefore, in the next step, heat transport through advection was incorporated into the model. To this end, regional faults and fractures were assumed to be the main conduits for fluid movement within the reservoir, and their influence in the thermal model is investigated through a series of conductive-convective simulations.

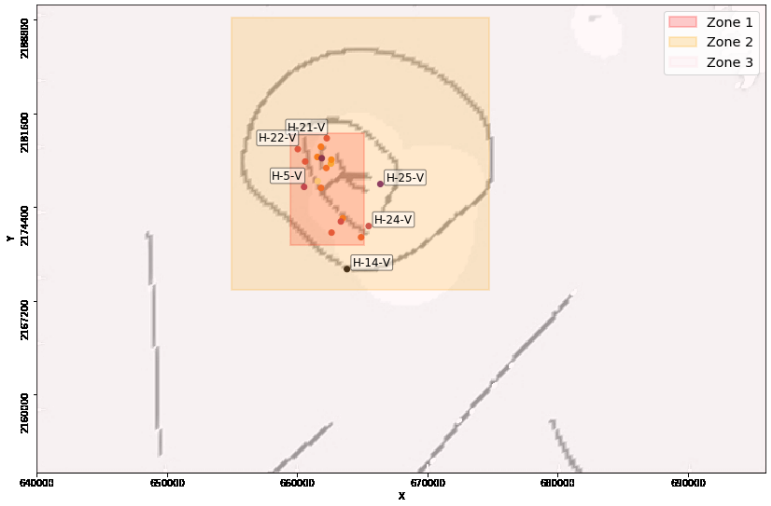

Figure 5: Regional heat flux configuration at 4600 m below sea level: Zone 1 – 0.35 W/m2, Zone 2 - 0.15 W/m2 and Zone 3- 0.091 W/m2, constrained using 3D conductive simulations.

3.4 Results

The numerical simulations were performed with particular focus on investigating the impact of unknown fault conditions in Los Humeros. The regional scale simulations aimed to investigate the influence of sealing conditions of the large caldera rim faults of Los Humeros and Los Potreros on the temperature field (Deb et al., 2019a), while in the reservoir scale simulations the impact of unknown permeability of the reservoir rocks and of the local faults and fractures controlling the fluid movement in the geothermal system was investigated (Deb et al., 2019c).

In this work, we present the results of the reservoir model which had the lowest error when compared with stabilized borehole temperature data (Figure 6). We calculated the misfit between simulated and bottom hole corrected temperature to evaluate the fitness of the model to represent the initial state (Figure 7). The simulation results underestimate the temperature measurements and a misfit of 20 – 30 % is observed in most of the wells. However, it should be noted that the temperature data in Los Humeros wells are significantly affected by convective flow in wells through the feeding zones especially due to boiling in many wells (H-8, H-16, H-17). Therefore, a perfect match between a steady-state simulation and the well temperatures cannot be expected. However, some interesting conclusions from the simulation results are as follows:

1. In the central-west zone (high temperature zones in the temperature maps of Figure 6), where the E-W faults intersect the N-S faults, development of strong convection cells are observed. This is also where most of the productive wells are located. Interestingly, there are also several dry and non-economic wells such as H-5, H-22, H-11 among others, located in this zone. This observation shows that the productivity of the wells is therefore not only

related to their location close to the heat source, but also if they encountered faults or nearby fault related damaged zones.

2. Towards the south and south-eastern corner, a general decline of temperature is observed. This is in accordance with the temperature observed in well H-14 and H-18 in the south (see Table 1 for BHT of wells).
3. The conceptual model of Los Humeros field, so far, regarded the heat source as a single cooling, partially crystallized magma chamber. The temperature data in the wells however suggest presence of localized heat anomaly sources. In the future work, these shallow heat sources shall be studied in more details.
4. The boiling process indicated by the temperature and pressure data is a result of production and insufficient recharge to the geothermal system. In our model, the main recharge is expected to take place through vertical infiltration within the caldera through the high porosity post-caldera volcanic deposits (Unit 1 and Unit 2). However, recent isotopic studies have indicated possible distal recharge (GEMex, WP 4, personal communication) through the highly-fractured over-thrusted sedimentary sequence of limestones, which may act as preferential pathways if connected through regional fault planes.

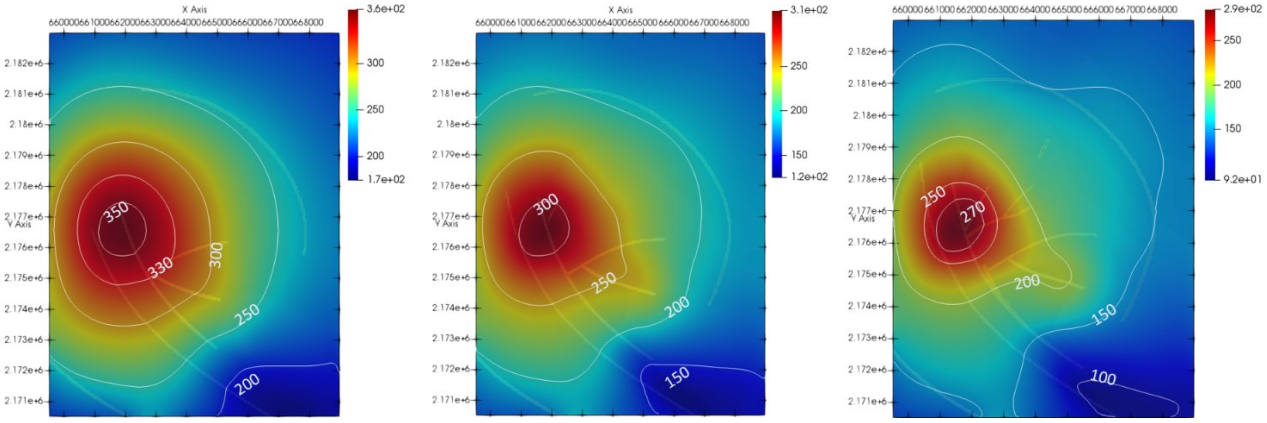

Figure 6: Temperature maps extracted at -100 m below sea level (left), 500 masl (center) and 1000 masl (right).

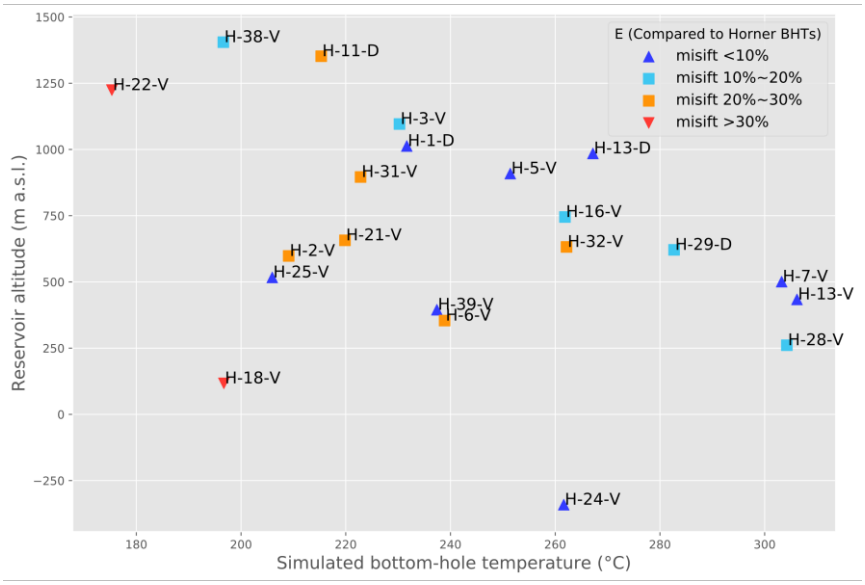

Figure 7: Mismatch between the simulated temperature and the bottom hole temperature in wells.

4 Modeling the brittle-ductile transition

The following contribution is an extract from Parisio et al. (2019) and covers the modeling approach for deformation and failure mode transition from brittle-cataclastic-localized patterns into ductile non-localized plastic-flow. The deformation mode is a function of temperature and mean stress (Byerlee 1968; Evans and Wong, 1990; Karato 2012) and it is particularly important in high temperature geothermal environments, where the geothermal gradient can exceed $90\ \mathrm{K\,km^{-1}}$ and alter the mechanical properties of rocks at shallower depth than in the cold crust. Lithology is another control on mechanical properties and the depth of the Brittle-Ductile Transition (BDT) differs for sedimentary or igneous and metamorphic rocks. Brittle failure is usually associated with dilatancy, crack nucleation, growth and propagation while the mechanical properties of strength and stiffness degrade rapidly with load increments. Ductile failure instead shows compaction or isochoric diffused deformation promoted by time-dependent solid-state diffusion (creep).

We have developed a constitutive model based on experimental evidence from literature on two rocks lithologies, a carbonate from Italy, Comiso Limestone (Bakker et al., 2015), and a basalt from France, Escandorgue Basalt (Violay et al., 2012). The experiments are obtained from published results of triaxial tests at high temperature and high pressure. Although both rocks are not from Los Humeros reservoir, they are assumed here to be analogues of the lithologies forming the reservoir and the basement. The tests are chosen because of the very wide temperature and stress range and due to the fact that an analogous dataset for LH samples is not available (i.e., high-temperature and high-pressure strength tests on LH lithologies). A limit surface (yield function) in the stress-temperature space provides the onset of inelastic deformations and represents the strength envelope of the material.

4.1 Static constitutive model

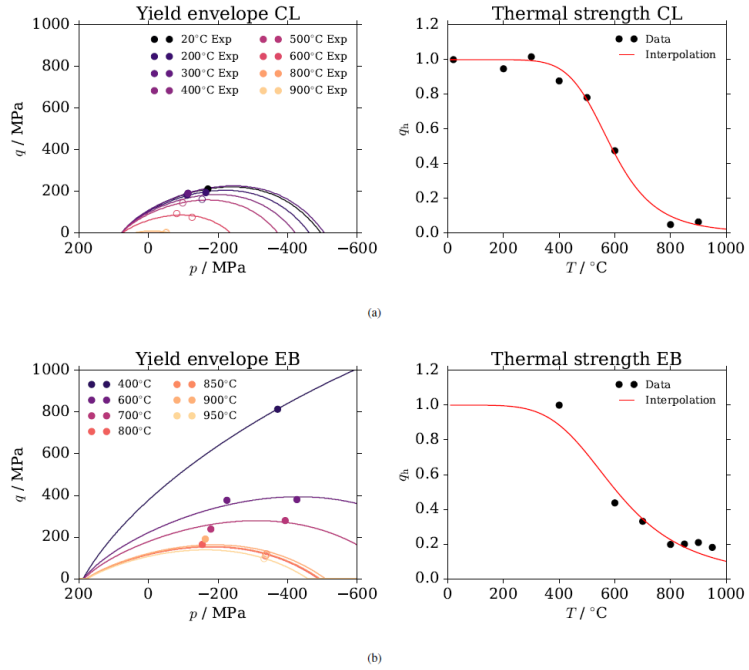

Figure 8: Calibration of the yield surface and thermal degradation function against experimental result.

The general framework of rate-independent plasticity is adopted and the plastic surface f_p is formulated in Biot's effective stress space $\sigma' = \sigma + \alpha_b p_w I$, with σ the total stress tensor, p_w the pore water pressure, α_b Biot's coefficient (assumed to be equal to 1) and I the second-order identity tensor. The solid mechanics sign convention is applied throughout this study, i.e., tensile stresses and strains are positive. The loading-unloading conditions are defined as $f_p(\sigma', T) \leq 0$, $\dot{\lambda} \geq 0$ and $\dot{\lambda} f_p(\sigma', T) = 0$, where $f_p(\sigma', T)$ is the temperature and stress-dependent yield surface and $\dot{\lambda}$ is the plastic multiplier (Parisio et al., 2019). The plastic multiplier defines the magnitude of the rate of plastic strain $\dot{\epsilon}_p = \dot{\lambda} \partial g_p / \partial \sigma'$, which is normal to the plastic potential surface g_p. If $g_p = f_p$, as it is assumed in our work, the plastic potential is said to be associated and the plastic strain rate tensor is normal to the yield surface f_p. The yield surface is defined in the effective stress space via the mean effective stress and deviatoric stress invariants p and q defined as

$$p = \frac{1}{3} tr(\sigma') \; q = \left(\frac{3}{2} s : s \right)^{\frac{1}{2}},$$

with the deviatoric effective stress tensor $s = \sigma - tr(\sigma) I/3$. The yield surface writes

$$f_p(p, q, T) = \left[\left(1 - q_h(T)\right) \left(\frac{q}{3\sigma_c} + \frac{p}{\sigma_c} \right)^2 + \frac{q}{\sigma_c} \right]^2 + m_0 q_h^2(T) \left(\frac{q}{3\sigma_c} + \frac{p}{\sigma_c} \right) - q_h^2(T),$$

where σ_c is the uniaxial compressive strength, m_0 a frictional parameter and $q_h(T)$ is an internal functional dependent on temperature that defines the opening of the yield surface toward higher confinements, is bounded in the interval $[0,1]$ and has the following expression

$$q_h(T) = \frac{q_p(\epsilon_p)}{[1 + (\alpha \Delta T)^n]^{\left(1-\frac{1}{n}\right)}}.$$

where $q_p(\epsilon_p)$ is a proper plastic hardening descriptor dependent on the plastic strain tensor ϵ_p. In the present case, $q_p = 1$ at the peak of stress (strength envelope) and $q_p = q_{p0}$, with $0 \leq q_{p0} \leq 1$, at the onset of inelasticity (yield envelope). $\alpha$and$n$ are material parameters defining the shape of thermal weakening. The yield envelope corresponds to the points in the stress-strain triaxial curves in which the behaviour becomes inelastic and the calibration against experimental evidence is shown in Figure 8. Further details of the calibration process can be found in Parisio et al. (2019). Within the adopted framework, in brittle conditions the inelastic deformation is dilatant and in ductile conditions it is instead compactant, in agreement with previous studies (Wong and Baud 2012; Parisio et al., 2019). Assuming the same convention, and assuming associated plasticity, the volumetric component of the inelastic deformation is $\dot{\epsilon}_{v,p} = \dot{\lambda} \partial f_p / \partial p$. The final values of the parameters of the model are reported in Table 4.

Table 4: Model parameters for the rocks under consideration.

Parameter	Comiso Limestone	Escandorgue Basalt	Unit
σ_c	293.8	807.5	MPa
m_0	3.857	4.309	
q_{p0}	0.5090	0.8161	
α	0.001781	0.001782	K^{-1}
n	7.599	4.968	-

The BDT depth is computed assuming a stress profile from the previous analyses, i.e., $24.5\ MPa/km$ of vertical stress, $25\ MPa/km$ of minimum horizontal stress and $50\ MPa/km$ of maximum horizontal stress. Pore pressure is computed as a hydrostatic water column having density that depends on temperature and pressure. The temperature profile is assumed as bi-linear approximation following Figure 9, with a maximum temperature set to $1050\ °C$. The lithology is simplified as a 2 km upper layer made of basalt and a basement made of limestone.

At a given depth z, temperature T, total σ and effective σ' stress tensors are known so that the acting mean effective $p_a{}'$ and deviatoric q_a stresses can also be computed; for a given pair $(p_a{}', T)$, the available deviatoric strength q^- and the deviatoric to volumetric component ratio of plastic strain rate $\dot{\epsilon}_{v,p}/\dot{\epsilon}_{D,p} = \left[\left(\partial f_p/\partial p\right)/\left(\partial f_p/\partial q\right)\right]_{p_a,q^-}$ are computed. Finally, the mobilized strength $\mu = q_a/q^-$ and dilatancy coefficient $\psi = arctan\left[\left(\partial f_p/\partial p\right)/\left(\partial f_p/\partial q\right)\right]_{p_a,q^-}$ are calculated.

4.2 Results

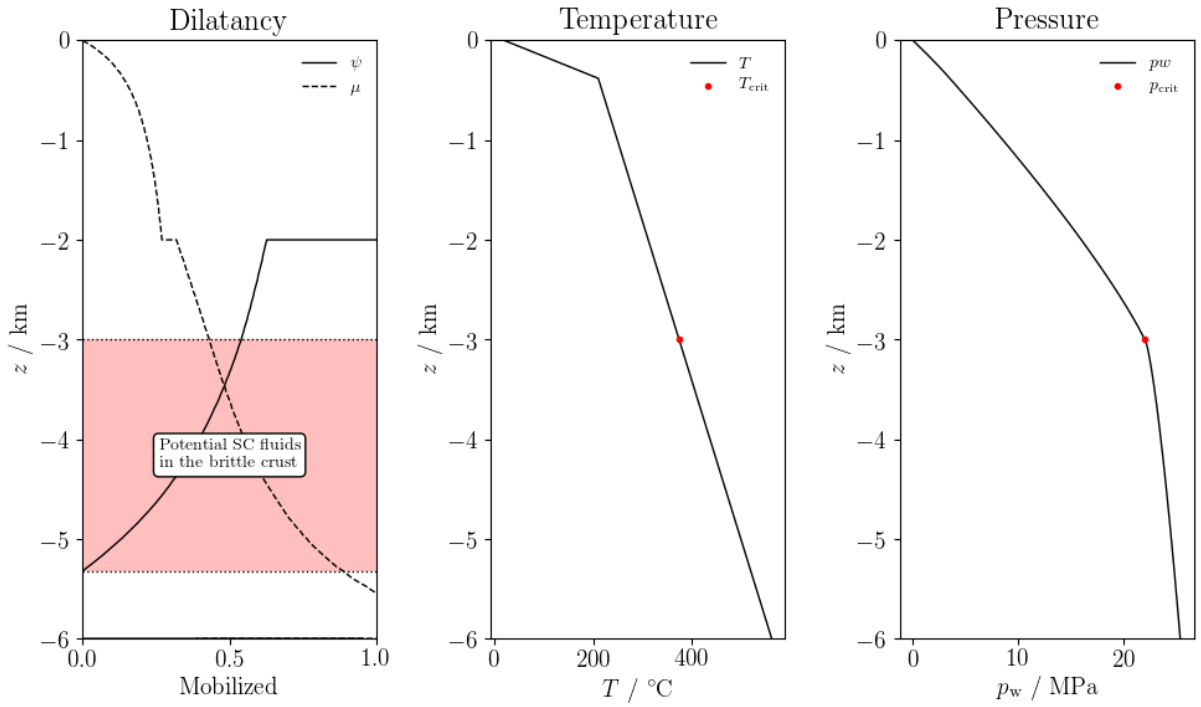

Figure 9: Mobilized dilatancy, strength, temperature and pressure with depth. The transition into supercritical fluids is found theoretically at around 3 km while the brittle regime extends up to slightly more than 5 km: in the range of 3-5 km depth supercritical fluids could be found in the fractured brittle crust at Los Humeros.

Figure 9 shows the mobilized dilatancy, mobilized strength, temperature and pressure with depth for an idealized case at Los Humeros. The depth of the BDT is located at approximately 5 km depth within the carbonatic basement. The model agrees with the observed natural seismicity that shows seismic attenuation below approximately 5.5 km (Jousset et al., 2019). The link between ductile deformation mode and a-seismic behaviour is known (Shimamoto and Noda 2014). The critical point (374 °C and 22.064 MPa) of the hydrostatic fluid column is located at approximately 3 km depth. From the model, we can estimate that at Los Humeros, it is possible that supercritical fluids can be present within the brittle rock at a depth between 3 to 5 km. The superposition of brittle deformation mode and supercritical fluid is particularly meaningful in terms of potential exploitation: in the brittle crust the relatively higher fracture frequency and permeability are likely to increase the natural permeability of the system, compared to the deeper parts in which the mechanical behaviour is ductile.

The model is built on a given set of hypotheses and does not take into account other factors, such as, e.g., the porosity-dependent strength (Heap et al. 2015; Schaefer et al. 2015; Wiesmaier et al. 2015). Furthermore, the model is calibrated on analogue rock lithologies from Los Humeros and better predictions require extensive high-temperature strength testing of rocks that are representative of the local formations.

4.3 Conclusion

Assessing the depth of the BDT is an important task in supercritical geothermal exploration: it can highlight the potential occurrence of supercritical fluids in brittle-fractured rock formation. In brittle regimes, rock form fractures that are more permeable than the porous structure and promote energy and mass transport for geothermal development. Predictions based on typical rock mechanical parameters yield a brittle behaviour up to roughly 5 km within the Los Humeros reservoir. A well drilled between 3 to 5 km has a good chance of finding supercritical fluids in the brittle crust, an ideal situation for supercritical geothermal development. Nonetheless, large uncertainties remain to be fully addressed on the geological structures at depth, on the state of stress, pore pressure and temperature below the current reservoir and on the high temperature strength properties of local lithologies. Additional investigation into these directions are necessary to better constrain the forecast on the brittle-ductile transition zone within the Los Humeros geothermal field.

5 Seismic response

The geophysical characterization of the Earth's subsurface is fundamental to monitor geothermal reservoirs and drill new wells. At high temperature and pressure, fluids could be in supercritical conditions and the rock in partially melted state. The seismic properties of porous formations, in terms of velocity, attenuation and dispersion are related to pressure and temperature conditions, which affect the behaviour of the rocks and of the saturating fluid. The full-waveform modelling jointly with information derived from available active-surface and passive seismic data and wells in the proximity of the active seismic lines has been used to evaluate and improve geophysical imaging and detection of the deep reservoir structures in the Los Humeros (Poletto et al., 2019; Jousset et al., 2019). Deliverable D5.5 (Poletto et al., 2019a) describes the results of the characterization of geothermal formations by full-waveform seismic modelling in poro-viscoelastic media saturated by fluids with temperature dependence.

5.1 Numerical simulation approach and method

Carcione et al. (2014) propose an algorithm to simulate full-waveform propagation using a stress–strain relation, including the effects of shear seismic attenuation and ductility due to shear deformations and plastic flow that takes into account the change from brittle to ductile behaviour of the rock. The method is based on the Burgers mechanical model that describes the anelastic behaviour through the effects of seismic attenuation and steady-state creep flow. The Burgers shear modulus $\mu_B(\omega)$ is function of the angular frequency ω. It is related to the in-situ stress through the relaxation times (τ_σ and τ_ε) of the unrelaxed shear modulus μ_0 and to the temperature through the shear viscosity (η)

$$\mu_B(\omega) = \frac{\mu_0(1 - i\omega\tau_\varepsilon)}{1 + i\omega\tau_\sigma - \frac{i\mu_0}{\omega\eta}(1 + i\omega\tau_\varepsilon)},$$

where $i = \sqrt{-1}$. The high temperature effects on seismic-wave losses are related to the Burgers viscosity and are solely due to shear deformations. The viscosity is related to the steady-state creep rate ($\dot{\varepsilon}$), which is in turn related to the absolute temperature (T) through the Arrhenius equation

$$\eta = \frac{\tau_0}{2\dot{\varepsilon}} = \frac{1}{2A_\infty}\tau_0^{1-n} exp\left(\frac{E}{RT}\right),$$

where τ_0 is the octahedral stress (Carcione and Poletto, 2013), used to describe the deformation of the ductile medium and is a function of the stress components along the principal axes and takes into account the effects of the deviatoric tectonic stress related to tectonic activity. The Arrhenius constants, characteristic of each material, A_∞ (MPa^{-n} s^{-1}) and n are a material constant and the stress exponent, respectively. E is the activation energy (J/mole) and R is the universal gas constant. The P-S and SH equations of motion can be recast in the velocity-stress formulation, including memory variables to avoid the computation of time convolutions. The equations correspond to isotropic anelastic and inhomogeneous media and are solved by a direct grid

method based on the Runge–Kutta time stepping technique and the Fourier pseudo-spectral method (Carcione and Poletto, 2013; Carcione et al., 2014).

Carcione et al. (2017) extended the study and the simulation algorithm to poro-viscoelastic media introducing the Gassmann equation to predict the low-frequency limit of the wet-rock bulk modulus, while the shear modulus of the wet-rock remains equal to the Burgers one. The saturated-rock Gassmann bulk modulus (K_G) depends on the porosity (ϕ) and the dry-rock (K_m), mineral grain (K_s) and fluid (K_f) bulk moduli

$$K_G = K_m + \alpha^2 M\,,$$

where

$$\alpha = 1 - \frac{K_m}{K_s}\,,$$

and

$$M = \frac{K_s}{1 - \phi - \frac{K_m}{K_s} + \phi\frac{K_s}{K_f}}.$$

The wave-propagation equations implemented by Carcione et al. (2017) allow us to simulate seismic signals in arbitrary isotropic anelastic and inhomogeneous media. They also present an example to show how anomalous conditions of pressure and temperature can in principle be detected with seismic waves.

5.2 Review of applications

The assessment of the rheological and of the temperature and pressure (T, P) conditions in geothermal areas is important to discriminate between variability in geophysical properties due to lithology and those related to thermal effects. The developed Burgers-Gassmann method can estimate not only the temperature effect on seismic properties, such as compressional- and shear-wave velocity, attenuation and dispersion, but also the fluid mass present in function of porosity and fluid phase. The study conducted with water can be modified to use geothermal fluids different from pure water. In addition to analytic evaluation, the calculation of synthetic full-waveform propagation in poro-viscoelastic formation is useful to improve the interpretation of existing acquisitions, as well as to predict the results of new seismic acquisitions, thus to design and optimize acquisition design and parameters, especially for exploration purposes in the perspective of drilling new wells.

We provide a review of the published works describing the method approach introduced in the previous chapter and some applications. Poletto et al. (2018) study the sensitivity of seismic-wave propagation properties assuming a temperature gradient model. At low seismic frequencies they analyse the trends of rock seismic properties (velocity, elastic moduli and attenuation) as function of temperature and their sensitivity to temperature variation. They also extend the poro-viscoelastic model to include the permeability.

Figure 10 shows the effects of temperature on the rock seismic velocities with and without the presence of geothermal fluid including the possible effects of pressure on the bulk and shear moduli of the dry rock and the possible presence of melted material and fluid in supercritical conditions.

At given temperature and pressure conditions, they consider a uniform formation and perform several analyses to observe the variation of the seismic properties in relation to the fluid density and bulk modulus, permeability and possible squirt flow effects and concluded that:

- The presence of melting leads to the decreasing of seismic velocities, in particular it affects the shear velocity which decreases toward zero (Figure 10, decreasing in the "Melting zone").

- The presence of geothermal fluid can be observed in the seismic velocities trends (see in Figure 10 the difference between curves without fluid $\phi = 0$, and with fluid $\phi = 5\%$).

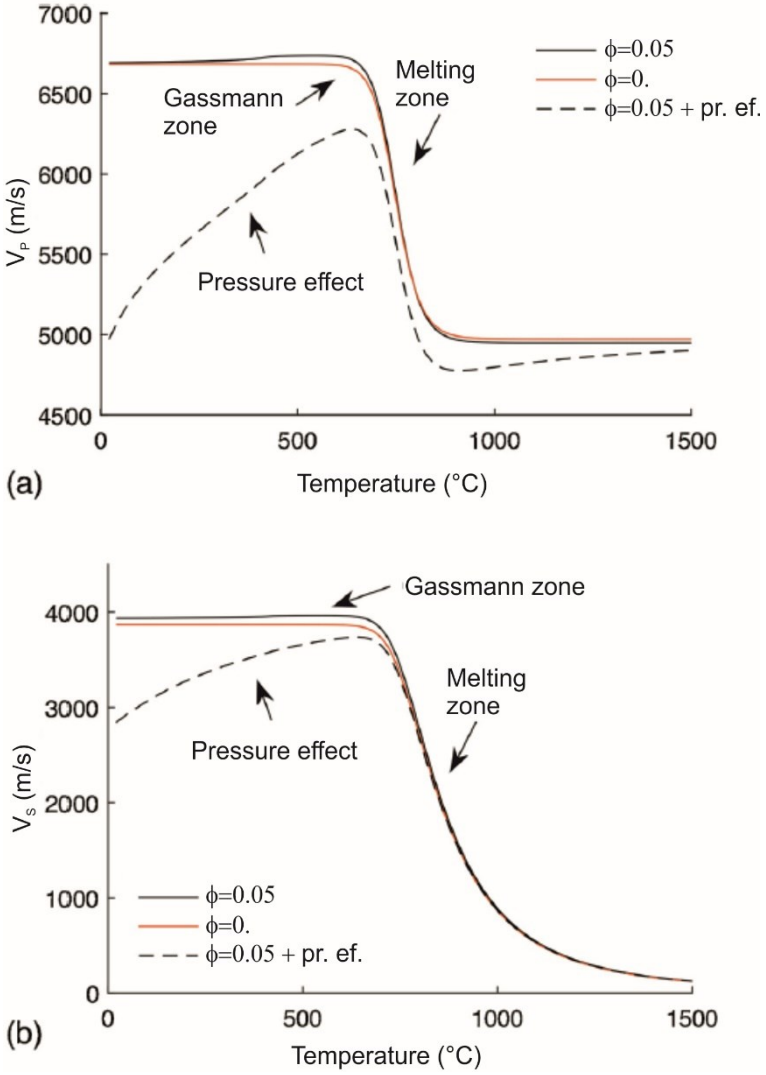

Figure 10: (a) P-wave velocity and (b) S-wave velocity versus temperature: without (ϕ=0) and with (ϕ=5%) geothermal fluid, including pressure effects (+pr.ef.). The variations due to the presence of fluid (Gassmann zone), the presence of melting (Melting zone) and the pressure effects are evidenced by arrows (after Poletto et al., 2018).

Note that in this analysis the authors observe that not always an increase in temperature correspond to an increase in seismic velocity in rocks (e.g., Mendrinos at al., 2019, D5.11), but the increasing or decreasing velocity trends depends on the regions selected in relation to their thermodynamic properties, as observed in the introduction of this section. They calculate the characteristic sensitivity curves for compressional and shear phase velocities using the Burgers-Gassmann poro-viscoelastic model at different conditions. There are observable variations in the curves after the inclusion of geothermal fluids with respect to the case where no (or negligible) porosity is assumed, including the supercritical zone at T>374°C (Figure 10). With bulk and shear moduli correction for pressure we observe effects and trends at low temperatures.

Farina et al., 2019 applied the method to calculate the seismic velocities and attenuation in geothermal areas in terms of the subsurface distribution of the confining and pore pressures and temperature, assuming that the heat transfer regime from below is either convective or conductive. In this analysis, the pore pressure is assumed as hydrostatic, with pure water as geothermal fluid. In hydrothermal systems the temperature is calculated assuming the boiling-point condition at the specific pore pressure within the reservoir. Beneath the reservoir it is assumed constant in convectively heated systems and following a constant temperature gradient in conductively heated systems. They focus on three application examples, considering simplified subsurface models to describe the geothermal systems beneath the geothermal wells assumed in the area.

- In the first example the authors consider a 3-layers 1D model based on crustal-rock geophysical and thermal parameters and observed the variation in the compressional and shear velocities and attenuation due to variation in temperature passing from the conductive to the convective heat transport regime. The fluid is in a vapour phase for both thermal models, and the fluid properties do not significantly change in the deeper part, even if the temperature difference reaches 400 °C. If the fluid is in a vapour state, variations in temperature results in small variations of the seismic velocities and quality factors of the saturated rock. For comparison, assuming constant petrophysical properties, they calculate the seismic properties of a geothermal reservoir considering the temperature and pressure of a convective liquid-dominated (LD) system where the temperature increases following the boiling-point to depth (BPD) curve until 1 km, where it reaches 300 °C and then it remains constant. The temperature variation that leads to change in the fluid state, from liquid to vapour, results in bigger variation of the seismic velocities with respect to the case in which the fluid state remains vapor. To investigate the changes due to variations of the rock properties, they focus on the deepest layer and vary only the Arrhenius parameters of the layer. They observed the corresponding variations in rock viscosity, seismic velocities and seismic attenuation as function of depth and as function of temperature. As discussed also in the following of this report, these geophysical variations may be potentially relevant for the characterization of the drilling context.
- In the second example the authors focus on the superhot geothermal system (SHGS) of Los Humeros. They consider a simple 1D model and starting from the temperature and

pressure information available from some of the wells located in the area, they extrapolate in depth assuming two heat transfer models, a conductive and a convective one. If the rock thermal properties (i.e., Arrhenius parameters) do not change. They observed that at the maximum temperature and pressure differences, the variability is about 0.2% for the seismic phase velocities and 2% for the seismic quality factors. If the thermal properties of the deepest layer are changed so that melting is allowed, instead, the maximum seismic phase velocity difference between the two analysed temperature–pressure conditions results 20%. In the latter case the potential implications for deep drilling are relevant (see next sections).

- In the third example the authors focus on the potential enhanced geothermal system (EGS) of Acoculco using a 1D model. Studies on the two drilled wells present in this area have shown that the temperature profile is linear, indicative of a conductive thermal regime. They assume a conductive model and change the thermal properties of the deepest layer, in terms of Arrhenius parameters, in order to analyse the seismic properties of a formation with and without melting at temperature greater than 700 °C. These examples have to be considered as preliminary results of the area in the perspective of further investigations and studies by in field geophysical measurements that will be available in the future.

Finally, in the third GEMex work, Poletto et al. (2019b) perform a full-waveform simulation using the geological and temperature model proposed by Verma et al. (1990) for Los Humeros (LH) super-hot geothermal system (SHGS). The authors study two scenarios. In the first they analyse the signals in the proximity of the melted formation calculating a synthetic vertical seismic profile (VSP) assuming a source at depth. They compare results obtained with melting and no-melting conditions, and observe differences in the predicted signals, namely up-going wave-fields, which can be interpreted from shallower positions before reaching the melting zone. In the second scenario they use the same rheological geometry and model with and without the presence of hot (with respect to the background zone) chimneys. They simulate wave propagation using a source in depth in a lateral position with respect to one of the chimneys and receivers at the surface in order to have synthetic waves travelling through the hotter chimney. The variation in the simulated waveform with and without hotter chimney is due to the rock properties variation, from solid to fluid transition, related to the change in temperature.

The simulation provides an analysis tool and makes it possible to detect differences in the seismic wavefields due to temperature effects, in surface and borehole measurements. Obviously, the repeatability conditions obtainable by synthetic data are not obtainable in nature, and the approach has to be adapted for full-waveform analysis of seismic data, with comparison and calibration of synthetic data and real measurements of deep structures.

5.3 Extension of the analysis on formation properties

In the following we present some characteristic examples. Theory as well as calculation of full-waveform examples can be further developed, and are outside of the scopes of this work. As we observe the BDT, we review the velocity curves and attenuation, with particular attention to the VP/VS ratio, and even more to the related Poisson ratio.

In the first example after simply scaling velocity, we use the same Arrhenius parameters and curves of Poletto et al. (2018). As shown in Figure 10, in the total melting region, V_S tends to zero and V_P/V_S tends to infinity. Figure 11 and Figure 12 show the trends of V_P/V_S versus temperature with a linear and a logarithmic plot. The last one is more efficient to evaluate the starting zone of the melting effect.

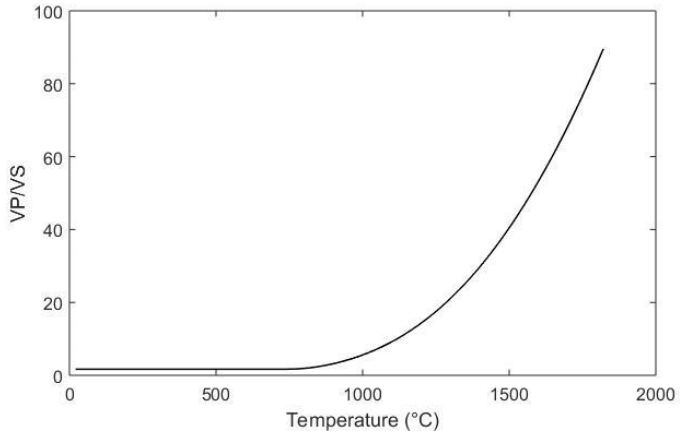

Figure 11: According with the V_S=0 property in the liquid melted region, the Poisson ratio tends to infinity: linear plot.

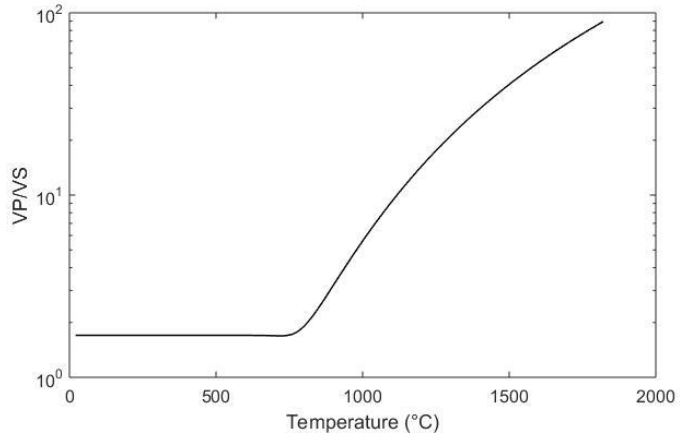

Figure 12: According with the V_S=0 property in the liquid melted region, the Poisson ratio tends to infinity: logarithmic plot.

In this analysis, in addition to the ratio V_P/V_S we use also the dimensionless Poisson coefficient that can be expressed as

$$\nu = \frac{\left(\frac{V_P}{V_S}\right)^2 - 2}{2\left(\frac{V_P}{V_S}\right)^2 - 2}.$$

The Poisson ratio, meaningful for the characterization of elastic properties of rocks, expresses the ratio of the transversal deformation and longitudinal deformation in the presence of a longitudinal solicitation. Its value ranges between -1 and 0.5. In the liquid where the shear velocity is zero, the Poisson coefficient is 0.5. The Poisson coefficient versus temperature (Figure 13) can be used to evaluate the variation in the rock properties due to the increase of partial melt fraction (e.g. Lay, Garnero and Williams, 2004).

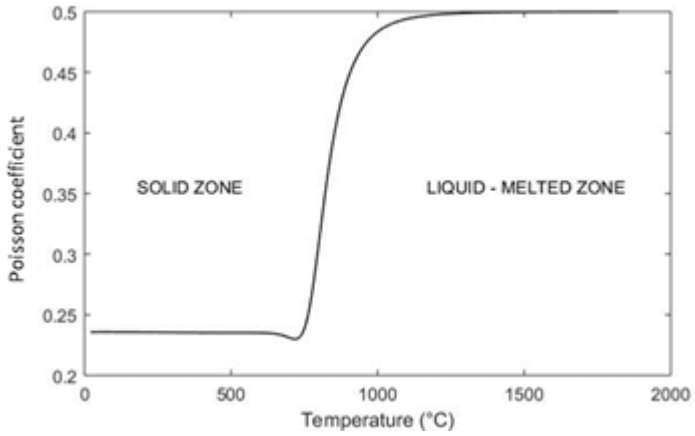

Figure 13: Plot of the Poisson coefficient versus temperature. This plot is effective to evaluate the variation in the rock properties due to melting, with a transition from solid-like to liquid-like status.

5.4 Implications for drilling parameters

Rock rheology is an important parameter affecting the drillability like, e.g., in percussion drilling. The penetration rate of percussive drills depends on the rock density, dynamic Young's modulus, shear modulus, longitudinal velocity, shear velocity and Poisson's ratio (Kahraman et al., 2003). All these quantities can be derived from VP, VS and density and correlated to seismic measurements. Kahraman et al. (2003) observed that, in particular compressive strength and those properties highly correlated with it, such as tensile strength and Young's modulus, exhibited good correlations with penetration rate. Dynamic elastic rock properties including the Young's modulus

$$Y = 2\rho V_S \frac{3V_P^2 - 4V_S^2}{V_P^2 - V_S^2},$$

and Poisson's ratio v are calculated in relation with the rock density, and compression and shear wave velocity, Vp and Vs. The dynamic properties representing log acquired data are converted to the static rock properties in static conditions (Archer and Rasouli, 2012).

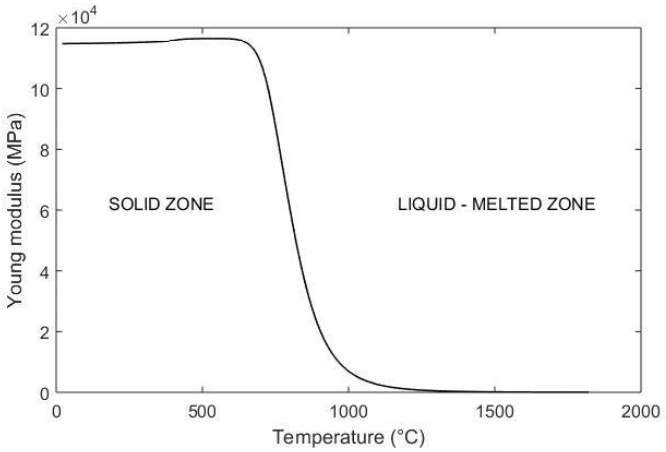

Figure 14: Plot of the dynamic Young's modulus versus temperature .

The variation of the dynamic Young's modulus in high temperature and melting zones is shown in Figure 15. This variation has implications for drillability conditions, as when the drilling depth approaches and reaches the melting-magma zone, and provides information useful to evaluate and optimize the drilling plan. Moreover, the phases of the drilling can be monitored with the seismic while drilling (SWD) technology that uses the drill-bit signal as seismic source and provides information on the formation ahead of the bit at almost all the depth levels of the well, as explained in the deliverable D8.4 (Mendrinos et al., 2020, in preparation).

5.5 Conclusions

These examples show that observable seismic variations can be expected in geothermal areas at relatively deep confinement conditions. The observation of these seismic variations still poses some questions on how reliable measurements can be obtained with sufficient precision in the subsurface at high depths in super-hot geothermal reservoirs. Here, high temperatures make it very difficult to measure by sensors in boreholes, and the depths of the local natural micro-earthquake sources are limited by the BDT. A variety of active and passive measurements has been considered in the framework of the GEMex project to detect deep structures, including seismic wavefields. As demonstrated by the analysis described in this report, these can be potentially useful, under certain boundary conditions, to provide information directly useful for drilling, or to indirectly provide precious information on nearby heat recharge zones, as well as information on expected rock quality.

6 A semi-analytic time-resolved poro-elasto-plastic model for wellbore stability and stimulation

The physical behaviour of the high-temperature reservoirs that the GEMex SHGS study is targeting (WP8) is a complex problem. As a result, problems can be expected while drilling into this reservoir. A major issue is the stability of wells during and after drilling. Unstable wells pose a major economic risk in the oil and gas industry – risks that can be reasonably expected to be larger in superhot geothermal systems. Some issues are: (i) large temperature differences due to cooling with the drilling fluid or after drilling with injection of cold water; (ii) elastoplastic constitutive behaviour of the high-temperature rock; and (iii) complex tectonic setting of the target rock. For wellbore stability evaluations and the associated decision-making process, good predictive tools are required. These tools, furthermore, need to be fast enough to be able to function in a probabilistic workflow: quality decision making requires the evaluation of many scenarios and sensitivities. Their quality and reliability, however, must be safeguarded by more elaborate or comprehensive models.

6.1 Approach

A major ingredient of a possible modelling approach to wellbore stability in SHGS is the coupling of thermal and mechanical behaviour, and, when fluid is injected, the hydraulic behaviour. Chemical issues of scaling, precipitation, solution, acid reactions and others can also play a role, but we have not yet incorporated them in our approach to date.

An extensive body of literature can be found on fast coupled subsurface models. For instance, fully transient analytical coupled models provide insight in the temporal development of stresses and pressures upon injection or production in a linear poro-elastic medium (Rice and Cleary, 1976). In another example, Tao and Ghassemi (2010) showed how thermoelastic coupling can affect strength due to temperature variations. The fast models that fundamentally account for time-dependent behaviour, however, generally do not incorporate non-elastic behaviour like failure or plasticity.

Other models do incorporate failure and plastic behaviour. As an example, Han and Dusseault (2003) assessed changes in porosity and permeability based on elastic – perfectly plastic behaviour. However, approaches in this line of thought usually employ steady-state pressure and temperature distributions or employ a simplified elastic – perfectly plastic scheme or an elastic – brittle – perfectly plastic scheme. Researchers having worked on more advanced constitutive models usually consider less coupling.

Fundamental problems remain when applying these models to the problems sketched above. The transient models do not incorporate plasticity. The plasticity models on the other hand are not rigorously transient and they do not incorporate continued plastic flow. They take the pressure field as static and base their treatment on a steady-state situation. This is not realistic, as injection or production induces changing pressures and temperatures and associated stresses. Neither of

the two model classes can assess incremental plasticity, variable injection rates, well shut-in, or flowback. An engineering tool must incorporate such features to be applicable to realistic scenarios.

The goal of this work aims at filling such gaps. We have developed a semi-analytical model in which the time-dependent behaviour is treated with an incremental setup. It mimics loosely coupled numerical models, in the sense that the output of hydro-thermal calculations constitutes the input of mechanical calculations in a time-sequential manner (Settari and Walters, 2001; Taron and Elsworth, 2009). Plastic behaviour is one of its fundamental ingredients, along with the time-dependent pressure and temperature development. The setup enables to address all the issues listed above, including progressive failure. Current limitations include the radial symmetry, a plane-strain stress solution, and an elastic-perfectly plastic constitutive model. We are addressing the issue of more advanced plastic models in ongoing research and intend to report on the results in the near future.

6.2 Model

We are interested primarily in the transient behaviour of wells completed over a considerable interval. Therefore, we have formulated our treatment for radial symmetry and for plane-strain conditions. We have treated the rock as a single-porosity medium with effective properties characterizing its behaviour.

Before the start of cooling or injection, a distortion of the in-situ stress field already exists due to the presence of the well and the inner boundary conditions on it. Indeed, the radial stress in the formation at the well radius of an open hole must equal the internal fluid pressure. The elastic solution that is available for this situation may not be appropriate, however: failure can occur in the formation around the well when a failure criterion is exceeded. We employ a Mohr-Coulomb criterion which presumes failure once the shear stress on a plane exceeds a linearly increasing function of the normal stress in the same plane. Under the assumption that the most critical stress in the plastic zone is at the Mohr-Coulomb failure envelope, the radial distribution of horizontal stresses can be calculated. In the elastic region they follow linear elasticity. The plasticity radius is calculated based on the requirements of continuity of the horizontal radial stress at it and of the advance of the failure envelope at its elastic side. For the strains and displacements, Hooke's law is applied in the elastic zone; in the plastic zone a perfectly plastic flow rule is employed. The radial displacement must be continuous at the plastic-elastic interface – this constrains the integration constant present in the solution to the flow rule.

After the start of pumping, be it production or injection, the pressure and temperature fields around the well change. The effect of these changes on the mechanical behavior can be described using linear poro-thermo-elasticity if it falls in the elastic regime. Whether or not this is the case must be determined by adding the stress increment calculated with poro-thermo-elasticity to the actual stress and applying the failure criterion to the result. If failure is indicated, additional

plasticity is incorporated. All contributions are additions to the existing fields, which makes the treatment truly incremental.

The pore pressure is a key ingredient in the determination of the stress field. However, the pressure field development is coupled with the mechanical development. We start with the description of linear poro-elasticity (Rice and Cleary, 1976; Detournay & Cheng 1988; Tao and Ghassemi, 2010) to formulate the full transient diffusivity equation – it deploys a diffusivity constant different from the traditional one in which flow only is considered: the effect of the poro-mechanical response is incorporated. The diffusivity equation can be solved under the assumption that the boundary conditions are known and the parameters are constant. However, the parameters prevalent in the diffusivity equation are not constant. Therefore, we employ a semi-steady-state solution similar to the one by Grant and Bixley (2011) and Dake (1983). We use the value of the coupled diffusivity to estimate the radius up to which the pressure is disturbed; within this radius we calculate the pressure using fully developed flow equations. This enables easy incorporation of time-dependent and position-dependent values for the mobility as well as changing rates. Mobilities are changed according to the output of the mechanical calculations.

For the thermal calculations we assume that convection is controlling it. For a zone of limited height, this could be extended with diffusion into the bounding layers (Candela et al., 2018). With convection only, and assuming immediate thermal equilibrium between the fluid and the matrix, a step function in the temperature results. The size of the cooled region is determined by the amount of (negative) heat pumped into the reservoir and the heat capacities of the water and of the gross rock volume.

Our approach is truly incremental. At every timestep, new temperature and pressure fields are calculated with the updated transmissivities and amount of heat pumped. The pressure and temperature increments are translated into stress increments. First, an elastic response is determined. If indeed the stresses do not exceed failure, this response is adequate. For regions where failure is occurring, plastic flow calculations are deployed, giving elastic and plastic contributions to the stain and giving the incremental stresses. For a more complete description of our approach we refer to Fokker et al. (2020). They also provide a benchmark with a numerical tool.

6.3 Example results

We have applied our model to a typical case representative for the Los Humeros setting. Input parameters are provided in Table 5. We simulated a case in which stimulation by injection is followed by a period of shut-in, and a case where it is followed by flowback.

Figure 15 shows the results for stimulation with cold fluid. We see how cold-fluid intrusion causes a mobility decrease in the cooled zone. From the beginning, plastic deformation close to well causes mobility increase due to stimulation of the facture network by a change in effective stresses. Temperature reduction also causes the stress to reduce (smaller absolute values of the

tangential stresses; moving away from criticality). The code cannot yet handle tensile stresses so the reservoir properties were chosen to ensure compressive stresses at all times.

Figure 16 shows the result of the pressure falloff after stimulation. After cessation of injection, the pressure stabilizes, starting from the well. There is only a minor effect on stresses, strains, and criticality.

Figure 17 shows the results during production after stimulation. We see a reversal of the pressure trend. In the last timestep, the temperatures have returned to virgin temperatures. The mobility, the stresses, the criticality and the strains react accordingly. The stimulation that is seen in the increased mobility close to the well results mainly from the initial plastic response around the wellbore due to drilling the hole. An extension to also include real tensile failure of the rock and the associated fracture opening and flow stimulation has not yet been implemented.

Table 5: Input parameters for the example runs. "Stimulation" involves possible change of the permeability due to fracture opening and closure.

Shared parameters		
Description	Symbol	Value
Depth [m]	D	4000
Reservoir thickness [m]	H_{res}	200
Wellbore radius [m]	R_w	0.1
Reservoir permeability [md]	k	2
Viscosity at Reservoir Temperature [mPa.s]	$\mu_{T\text{-}res}$	0.1
Viscosity at Injection Temperature [mPa.s]	$\mu_{T\text{-}inj}$	0.34
Porosity [-]	ϕ	0.02
Virgin reservoir pressure [MPa]	P_0	40
Reservoir temperature [°C]	T_{res}	100
Injection temperature [°C]	T_{inj}	70
Water heat capacity [J/m^3°C]	C_{water}	$4.2*10^6$
Rock heat capacity [J/m^3°C]	C_{rock}	$3.0*10^6$
Reservoir Young's modulus [GPa]	E	27
Fluid bulk modulus [GPa]	K_{fluid}	2
Reservoir Poisson ratio [-]	ν	0.20
Reservoir linear thermal expansion coefficient [°C^{-1}]	α_B	$1.*10^{-5}$
Virgin horizontal stress [MPa]	σ_h	-64
Virgin vertical stress [MPa]	σ_v	-80
Biot coefficient [-]	α_{Biot}	1.0
Mohr-Coulomb friction coefficient [-]	μ_{MC}	0.57

Mohr-Coulomb cohesion [MPa]	S_0	2.0
Plastic dilation ratio [-]	ψ	0.10
Case ID	Stimulation and Pressure Fallof	Stimulation and Production
Q_{inj} [m^3/min]	0.08 – 0.0	0.08 – -0.04
t_q [days]	30 – 30	30 – 63

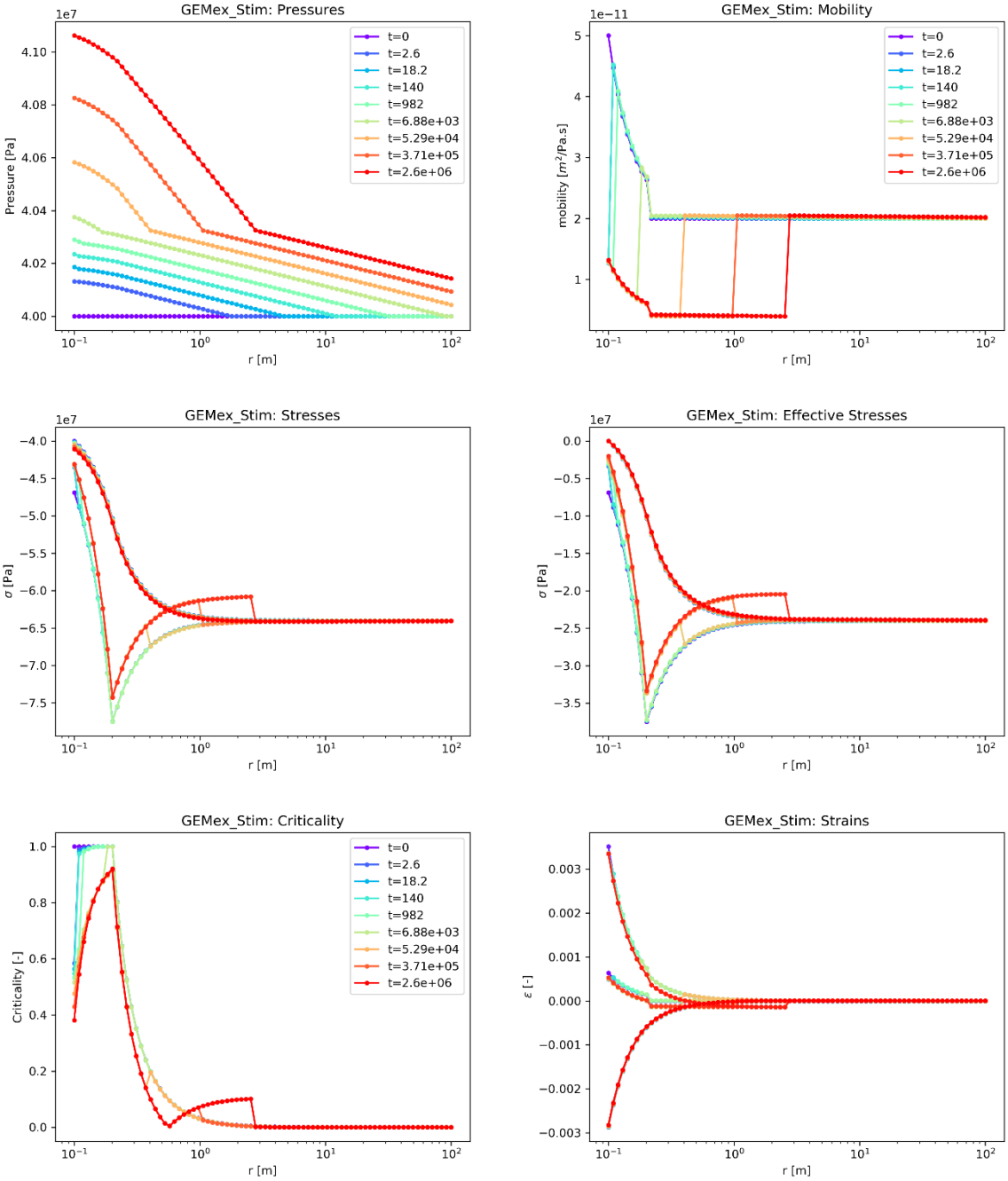

Figure 15: Stimulation with cold fluid. Pressures (top-left) and related mobilities (top right). The mobility changes result from temperature changes and from the induced effective stresses (middle row). The reservoir starts in a critical state close to the well and moves away from it due to pressurization and cooling (bottom left). The strains in the process (bottom right) are tensile (i.e. positive) radial and compressive (negative) tangential; adding up to tensile total strain.

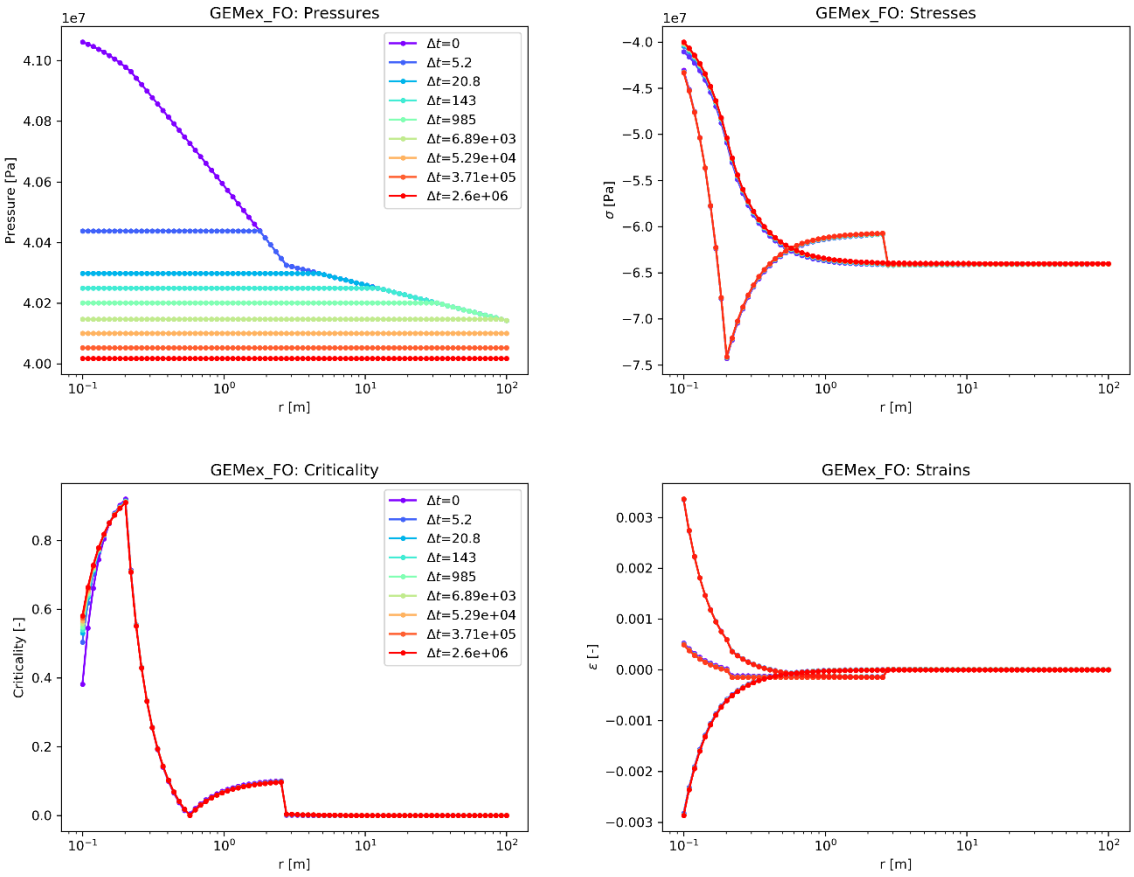

Figure 16: Pressure falloff after stimulation. Pressure stabilization (top left); minor development of the stresses (top right) and the criticality (bottom left); virtually stable strains (bottom right).

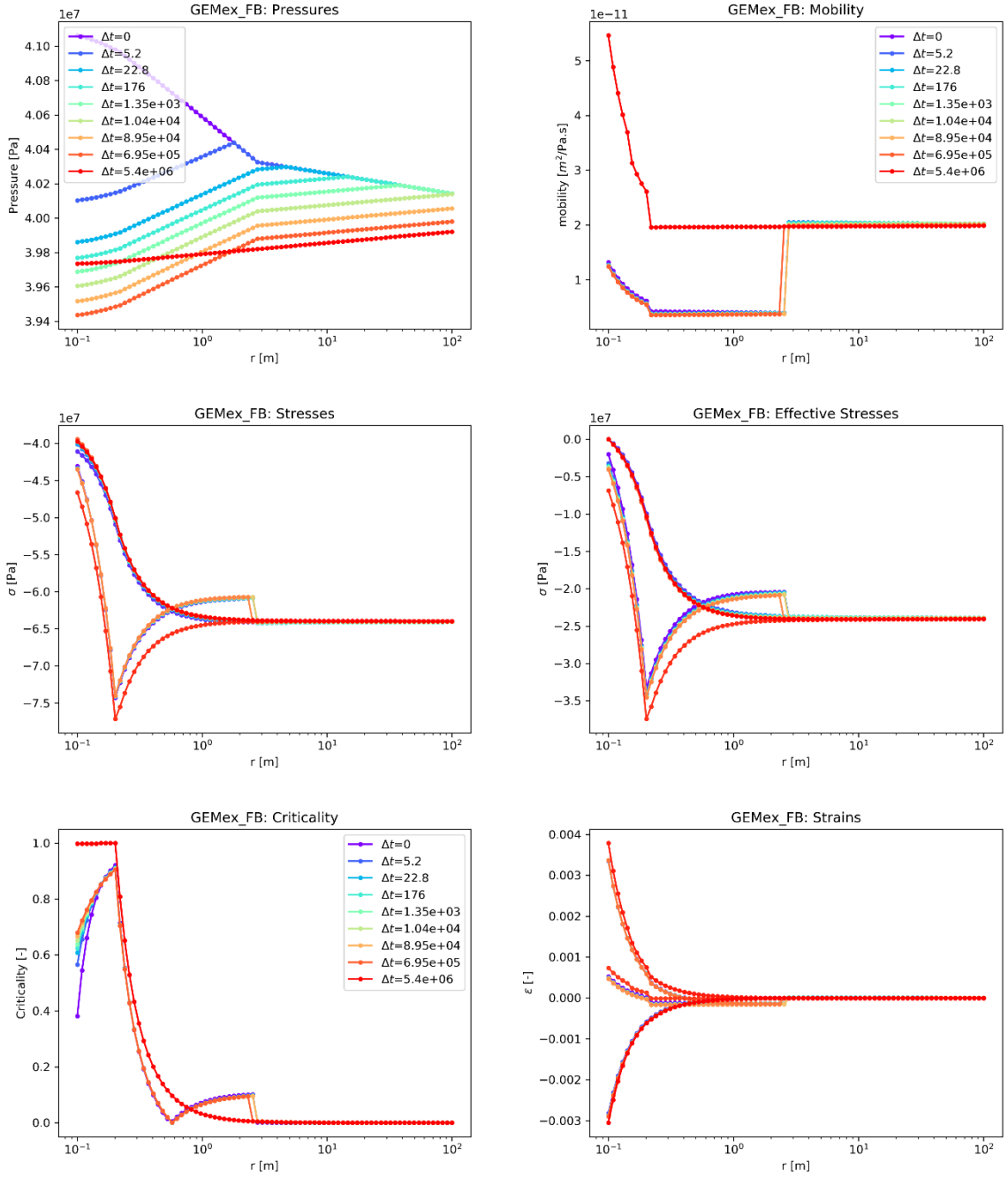

Figure 17: Production after stimulation. Reversal of pressure trend (top left). In the last timestep the mobility close to the well increases with the temperature increase (top right). The stresses also reverse to the original values (middle row). Criticality and strains react accordingly (bottom row).

6.4 Discussion

We have employed a plane strain approach in our model. Vertical stresses are calculated and they contribute to the mechanical response, but they have not been considered as essentially contributing to plasticity. The plane-strain approximation implies that the possible effect of a finite height of the layers in which the pressure and temperature disturbances occur is not incorporated. Different approaches can be envisioned to address these issues. For the incorporation of the

vertical stress, the start should be from the elastic response. If the combination of effective vertical and horizontal stress exceeds the failure criterion, plasticity may be employed to reduce the vertical stress. For the effect of a finite height, approaches like the one by Atefi Monfared and Rothenburg (2016) could be considered. They could be benchmarked with exact solutions available for cylindrical zones with constant temperature or pressure disturbance (Myklestad 1942; Perkins & Gonzalez, 1985; Candela et al., 2018).

In addition to the plane-strain approximation, we have limited ourselves to a radial symmetry. Any plastic zone is thus bounded by one or two radii of elastic-plastic transition (Han & Dusseault, 2003; Masoudian and Hashemy, 2016). An extension to non-radial symmetries would be very beneficial, in particular for strike-slip faulting regimes and for deviated wells. This, however, is a major effort since the equations complicate considerably. A possible approach is in the line of Galin (1946) and Detournay & Fairhurst (1987), who proposed solutions for limited stress ratios with forms of an elliptical yield zone around a circular cavity. However, a numerical approach may still be warranted, in particular when also the plane-strain approximation needs to be abandoned.

The examples we presented showed tangential stresses staying below the pore pressure: no dilatational stresses developed. Larger injection rates, smaller permeabilities or continued injection might result in such dilatational stresses. Then, fluidization might occur close to the wellbore, even with pressures well below the minimum in-situ stress. Such situations must be treated with models different from the simple elastic – perfectly plastic models that we employed here. We do not see fundamental difficulties on the way to such implementation.

Enhanced Geothermal Systems usually target low-permeability, fractured rock like granites or volcanic rock (Olasolo et al., 2016). For such systems, plasticity models may not be appropriate. Here, fracture network models can be employed. Rutqvist et al. (2013) give an example of such a model in the numerical domain. What is additionally required within our setup is the implementation of the mechanic response of the fracture network.

6.5 Concluding remarks

We have devised, implemented, tested and demonstrated a semi-analytic coupled poro-thermo-elasto-plastic model for wellbore stability and stimulation. As it fundamentally employs a sequential time-dependent scheme, it is optimally suitable for time-dependent plasticity, for tracking developing reservoir properties, and for operational scenarios with changing injection or production rates. Plastic behaviour can take place close to the wellbore, but also in isolated regions away from it. This depends on the specifics of the driving parameters. Our tool can be easily used in data assimilation workflows and in optimization. Further, it is ideal for assessing the large-scale effects of laboratory-derived models and of their driving parameters. Extensions envisaged for application to geothermal energy include thermal effects and more advanced plasticity models.

7 Conclusion

Drilling into supercritical reservoirs is a highly complex task that entails risk and uncertainties. The deep volcanic and magmatic environments are difficult to access and indirect methods are essential to provide estimates and scenarios before drilling operation can take place. In this sense, theoretical predictions that rely on physics-based models are essential. Reliable models are also fundamental to help the interpretation of complex geophysical observations, another key component in indirect methods. Additional complexity stems from the high temperature environment and the complex fluid-solid interactions of supercritical geothermal systems: this deliverable contains a series of methods that can be employed to make forecasts of possible drilling targets below the current geothermal reservoir at Los Humeros.

The state of stress in Los Humeros caldera is very complex and, although few measurements exist, well-log observations indicate a stress regime that fluctuates in space between strike-slip and reverse faulting regime. Numerical simulations of conductive heat transport have shown the non-uniform distribution of heat flow within the Los Humeros area and the role of faults in the geological heat transport processes. A model for the depth of the brittle-ductile transition was developed based on the theory of temperature-dependent plasticity. Within the given assumptions, the model estimates that an overlap between the possibly-fractured brittle crust and supercritical resources could be found between 3 to 5 km depth at the Los Humeros field. Complex models of temperature-dependent seismic wave velocity models have been developed by including plasticity and creep of the solid along with the full equations of state of the fluid. The methods are particularly useful to interpret seismic surveys and provide information about fluids states and the possible presence of partially melted materials. Indirectly, the model can provide information about drilling performance as a function of temperature. Finally, a coupled thermo-hydro-mechanical solution for wellbore stability has been developed based on Mohr-Coulomb plasticity theory. The model has advanced capabilities in estimating the wellbore integrity throughout the whole series of operations, from drilling through injection, testing, and production.

As for every model, shortcomings exist in terms of restrictive hypotheses. The models developed here are targeted for high-temperature environments and the hypotheses made are chosen in such a way that the main effects are not neglected. Additionally, any model is as good and as reliable as the data that is employed as input: predictions are at most as accurate as initial measurements. Nonetheless, the models can pin-point future development strategies and scenarios and can guide laboratory and in-situ investigations in a two-way feeding loop that is aimed at reducing uncertainty. Ultimately, drilling into a supercritical reservoir depends on the available resources, on the goals that are to be met and on the potential failure risks that operators are willing to take: the great amount of knowledge gathered during more than three decades of operations of Los Humeros geothermal reservoir and during the three years of GEMex project make it an ideal candidate for future development of the first supercritical geothermal wellbore in Latin America.

8 References

Archer, S., and Rasouli, V., (2012). A log based analysis to estimate mechanical properties and in-situ stresses in a shale gas well in North Perth Basin, in Kroshnaw, F.M. (ed), 1st International Conference on Petroleum and Mineral Resources.

Arellano, V. M., García, R.M., Barragán, G., Izquierdo, A., Araagón, A., Nieva, D., (2003). An updated conceptual model of the Los Humeros geothermal reservoir (Mexico), Journal of Volcanology and Geothermal Reserarch , 124, 67- 88.

Atefi Monfared, K., & Rothenburg, L. (2016). Poro-elasto-plastic response of an unconsolidated formation confined with stiff seal rocks under radial injection. International Journal for Numerical and Analytical Methods in Geomechanics, 40(13), 1799-1826.

Al-Ajmi, A. M., & Zimmerman, R. W. (2005). Relation between the Mogi and the Coulomb failure criteria. International Journal of Rock Mechanics and Mining Sciences, 42(3), 431-439.

Bai, M., & Abousleiman, Y. (1997). Thermoporoelastic coupling with application to consolidation. International Journal for Numerical and analytical methods in Geomechanics, 21(2), 121-132.

Bai, M., & Elsworth, D. (1994). Modeling of subsidence and stress-dependent hydraulic conductivity for intact and fractured porous media. Rock mechanics and rock engineering, 27(4), 209-234.

Bai, M., & Roegiers, J. C. (1994). Fluid flow and heat flow in deformable fractured porous media. International journal of engineering science, 32(10), 1615-1633.

Bakker, R. R., Violay, M. E. S., Benson, P. M., & Vinciguerra, S. C., (2015). Ductile flow in sub-volcanic carbonate basement as the main control for edifice stability: New experimental insights. Earth and Planetary Science Letters, 430, 533–541.

Bakker, R. R., Violay M.E.S., Vinciguerra S. C., Fazio M., and Benson P. M., (2019). Constitutive Laws for Etnean Basement and Edifice Lithologies. JGR Solid Earth, 124 (10), 10074-10088.

Bär, K., Weydt, L., Deb, P., Kummerow, J.,Ferrero, A., Vagnon, F., Colombero, C., Chicco, J., Vinciguerra, S., Siegfried, R., Comina, C., Mandrone, G., Laciska, A., Kemp, S., Kilpatrick, A., Rochelle, C., Milsch, H., Vacha, D., Rushton, J., (2019). Comprehensive report on the rock and fluid samples and their physical properties in the Acoculco and Los Humeros regions. GEMex – H2020 project report D6.1, https://data.d4science.net/zVLc

Bear, J. (1979). Hydraulics of groundwater New York. Mc GrawHill Inc.

Borja, R. I., Yin, Q., & Zhao, Y. (2019). Cam-Clay plasticity. Part IX: On the anisotropy, heterogeneity, and viscoplasticity of shale. Computer Methods in Applied Mechanics and Engineering, 112695.

Byerlee, J. D. (1968). Brittle-ductile transition in rocks. Journal of Geophysical Research 73, 4741–4750.

Candela, T., van der Veer, E. F., & Fokker, P. A. (2018). On the Importance of Thermo-elastic Stressing in Injection-Induced Earthquakes. Rock Mechanics and Rock Engineering, 51(12), 3925-3936.

Calcagno, P., Evanno, g., Trumpy, E., Gutiérrez-Negrín, L. C., Macías, J. L., Carrasco-Núñez, G., Liotta, D., (2018). Preliminary 3-D geological models of Los Humeros and Acoculco geothermal fields (Mexico) – H2020 GEMex Project., *Advances in Geosciences, 45,* 321 – 333.

Carcione, J. M., and Poletto, F., (2013). Seismic rheological model and refection coefficients of the brittle-ductile transition, Pure and Applied Geophysics, DOI 10.1007/s00024-013-0643-4.

Carcione, J.M., Poletto, F., Farina, B., Craglietto, A., (2014). Simulation of seismic waves at the Earth's crust (brittle–ductile transition) based on the Burgers model. Solid Earth Discuss. 6, 1371–1400.

Carcione, J.M., Poletto, F., Farina, B., Craglietto, A., (2017). The Gassmann–Burgers model to simulate seismic waves at the Earth crust and mantle. Pure Appl. Geophys. 174, 849–863. https://doi.org/10.1007/s00024-016-1437-2.

Carrasco-Núñez G., Arzate J., Bernal J.P., Carrera J., Cedillo F., Dávila-Harris P., Hernández J., Hurwitz S., Lermo J., Levresse G., López P., Manea V., Norini G., Santoyo E., Willcox C., (2015). A New Geothermal Exploration Program at Los Humeros Volcanic and Geothermal Field (Eastern Mexican Volcanic Belt), Proceedings World Geothermal Congress 2015, Melbourne, Australia, 19-25 April 2015.

Carrasco-Núñez, G., López-Martínez, M., Hernández, J., Vargas, V., (2017). Subsurface stratigraphy and its correlation with the surficial geology at Los Humeros geothermal field, eastern Trans-Mexican Volcanic Belt, Geothermics, 67, 1 – 17.

Chen, S. L., & Abousleiman, Y. N. (2013). Exact drained solution for cylindrical cavity expansion in modified Cam Clay soil. Géotechnique, 63(6), 510.

Chen, S. L., & Abousleiman, Y. N. (2018). Cavity expansion in strain hardening frictional soils under drained condition. International Journal for Numerical and Analytical Methods in Geomechanics, 42(1), 132-142.

Cedillo-Rodríguez, F. (2000). Hydrogeologic model of the geothermal reservoirs from Los Humeros, Puebla, Mexico. Proceedings World Geothermal Congress 2000, Kyushu – Tohoku, Japan, May 28 – June 10, 2000.

Clauser, C., ed., (2003). Numerical Simulation of Reactive Flow in Hot Aquifers. SHEMAT and PROCESSING SHEMAT, Springer, New York.

Dake, L. P. (1983). Fundamentals of reservoir engineering (Vol. 8). Elsevier.

Davis, R. O., & Selvadurai, A. P. (2005). Plasticity and geomechanics. Cambridge university press.

Deb, P., Knapp, D., Marquart, G., Montegrossi, G., (2019a). Report on the calibrated reservoir model for the super-hot reservoir at Los Humeros and its calibration against available field data. GEMex – H2020 project report D6.3 https://data.d4science.net/Tz4d

Deb, P., Knapp, D., Clauser, C., and Montegrossi, G., (2019b). Modeling natural steady- state of super-hot geothermal reservoir at Los Humeros, Mexico, European Geothermal Congress, Den Haag, The Netherlands, 11-14 June 2019.

Deb, P., Knapp, D., Marquart, G., Montegrossi, G., (2019c). Report on the calibrated reservoir model for the super-hot reservoir at Los Humeros and its calibration against available field data. GEMex – H2020 project report D6.6, https://data.d4science.net/xhNC.

Detournay, E., & Cheng, A. D. (1988, June). Poroelastic response of a borehole in a non-hydrostatic stress field. In International Journal of Rock Mechanics and Mining Sciences & Geomechanics Abstracts (Vol. 25, No. 3, pp. 171-182). Pergamon.

Detournay, E., & Fairhurst, C. (1987, August). Two-dimensional elastoplastic analysis of a long, cylindrical cavity under non-hydrostatic loading. In International Journal of Rock Mechanics and Mining Sciences & Geomechanics Abstracts (Vol. 24, No. 4, pp. 197-211). Pergamon.

Dowdle, W. L. and Cobb, W.M., (1975). Static formation temperature from well logs – an empirical method, Journal of Petroleum Technology 27 (11), 1326-1330.

Evans, B., Fredrich, J.T. and Wong, T.F., (1990). The brittle-ductile transition in rocks: Recent experimental and theoretical progress. The Brittle-Ductile Transition in Rocks, Geophys. Monogr. Ser, 56, pp.1-20.

Evensen, G. (2009). Data assimilation: the ensemble Kalman filter. Springer Science & Business Media.

Fjaer, E., Holt, R. M., Raaen, A. M., Risnes, R., & Horsrud, P. (2008). Petroleum related rock mechanics (Vol. 53). Elsevier.

Fokker, P.A. and B.B.T. Wassing (2019). A fast model for THM processes in geothermal applications. Presented at the European Geothermal Congress, 11 – 14 June 2019; The Hague, The Netherlands.

Friðleifsson, G.Ó., Elders, W.A., Zierenberg, R.A., Fowler, A.P., Weisenberger, T.B., Mesfin, K.G., Sigurðsson, Ó., Níelsson, S., Einarsson, G., Óskarsson, F. and Guðnason, E.Á., (2018). The Iceland Deep Drilling Project at Reykjanes: Drilling into the root zone of a black smoker analog. Journal of Volcanology and Geothermal Research.

Galin, L. A. (1947). Plane elastic-plastic problem: plastic regions around circular holes in plates and beams. Division of Applied Mathematics, Brown University.

Gaucher, E., Schoenball, M., Heidbach, O., Zang, A., Fokker, P. A., van Wees, J. D., & Kohl, T. (2015). Induced seismicity in geothermal reservoirs: A review of forecasting approaches. Renewable and Sustainable Energy Reviews, 52, 1473-1490.

Ghassemi, A. (2012). A review of some rock mechanics issues in geothermal reservoir development. Geotechnical and Geological Engineering, 30(3), 647-664.

Grant M.A., P.F. Bixley and LG. Donaldsson, (1983). Internal Flow in Geothermal Wells: Their Identification and Effect on the Wellbore Temperature and Pressure Profiles. J. Society Petroleum Engineers, pp. 168-176, May 1983.

Grant, M. A., & Bixley, P. F. (2011). Geothermal Reservoir Engineering. Academic Press.Han, G., & Dusseault, M. B. (2003). Description of fluid flow around a wellbore with stress-dependent porosity and permeability. Journal of petroleum science and engineering, 40(1-2), 1-16.

Gutiérrez-Negrín LCA, Quijano-León J.L. (2004), Analysis of seismicity in the Los Humeros, Mexico, geothermal field. In: Geothermal Resources Council Transactions, pp 467–472.

Heap, M.J., Farquharson, J.I., Baud, P., Lavallée, Y. and Reuschlé, T., (2015). Fracture and compaction of andesite in a volcanic edifice. Bulletin of volcanology, 77(6), p.55.

Heidbach O., Rajabi M., Reiter K., Ziegler M., WSM Team, World stress map database release 2016.

Hofmann, H., Zimmermann, G., Farkas, M., Huenges, E., Zang, A., Leonhardt, M., ... & Fokker, P.A. (2019). First field application of cyclic soft stimulation at the Pohang Enhanced Geothermal System site in Korea. Geophysical Journal International, 217(2), 926-949.

Horner D. R., (1951). Pressure buildup in wells, in Proceedings of Third World Petroleum Congress, Section II, The Hague, Netherlands, 28 May – 6 June.

Izquierdo, G., Arellano, V.M., Aragón, A., Portugal, E. and Torres, I., (2000). Fluid acidity and hydrothermal alteration at the Los Humeros geothermal reservoir, Puebla, México. Proc. World Geothermal Congress 2000, Kyushu-Tohoku Japan, May-June 2000, pp. 1301-1306.

Jaeger, J. C., Cook, N. G., & Zimmerman, R. (2007). Fundamentals of rock mechanics. John Wiley & Sons.

Jansen, J. D., Brouwer, R., & Douma, S. G. (2009, January). Closed loop reservoir management. In SPE reservoir simulation symposium. Society of Petroleum Engineers.

Jousset P., et al. (2019), Seismic structures of the Acoculco and Los Humeros geothermal fields, Version 1.0, GEMex Deliverable 5.3, Work package 5 – Task 2.

Kahraman S., Bilgin N., and Feridunoglu C., et al., (2003). Dominant rock properties affecting the penetration rate of percussive drills. International Journal of Rock Mechanics & Mining Sciences, 40, 711-723.

Karato, S.-i (2012). Deformation of earth materials: an introduction to the rheology of solid earth (Cambridge University Press, 2012).

King, G. E. (2010, January). Thirty years of gas shale fracturing: What have we learned?. In SPE Annual Technical Conference and Exhibition. Society of Petroleum Engineers.

Kruszewski, M. and Wittig, V., (2018). Review of failure modes in supercritical geothermal drilling projects. Geothermal Energy, 6(1), p.28.

Kutasov, I.M., and Eppelbaum, L.V. (2005). Determination of formation temperatures from bottom-hole temperature logs - a generalised Horner method, Journal of Geophysics and Engineering, 2, 90 - 96, doi:10.1088/1742-2132/2/2/002.

Lay T., Garnero E. J., and Williams Q., (2004). Partial melting in a Termo-Chemical Boundary layer at the base of the mantle. Physics of the Earth and Plan. Int., 146 (3), 441-467.

Lee, K. K., Ellsworth, W. L., Giardini, D., Townend, J., Ge, S., Shimamoto, T., ... & Chang, C. (2019). Managing injection-induced seismic risks. Science, 364(6442), 730-732.

Lermo J., Antayhua Y, Quintanar L, Lorenzo C., (2007), Estudio sismológico del campo geotérmico de Los Humeros, Puebla, México. Parte I: Sismicidad, mecanismos de fuente y distribución de esfuerzos. In: Congreso Anual 2007.

Lermo J., Lorenzo C., Antayhua Y., Ramos E., Jiménez, N. (2016), Sísmica pasiva en el campo geotérmico de Los Humeros, Puebla-México y su relación con los pozos inyectores. XVIII Congreso Peruano de Geología, pp. 1–5.

Lermo, J., Antayhua, Y., Quintanar, L. and Lorenzo, C. (2008), Estudio sismológico del campo geotérmico de Los Humeros, Puebla, México. Parte II. Revista Mexicana de Geoenergía.

Liu, J., Fokker, P. A., & Spiers, C. J. (2017). Coupling of swelling, internal stress evolution, and diffusion in coal matrix material during exposure to methane. Journal of Geophysical Research: Solid Earth, 122(2), 844-865.

Lorenzo-Pulido C.D., Borehole Geophysics and Geology of Well H-43, Los Humeros Geothermal Field, Puebla, México, Reports of Geothermal Training Programme, United Nations University, Orkustofnun, Grensásvegur 9, IS-108 Reykjavík, Iceland, Reports 2008, Number 23, 2008.

Lu, S. M. (2018). A global review of enhanced geothermal system (EGS). Renewable and Sustainable Energy Reviews, 81, 2902-2921.

Masoudian, M. S., & Hashemi, M. A. (2016). Analytical solution of a circular opening in an axisymmetric elastic-brittle-plastic swelling rock. Journal of Natural Gas Science and Engineering, 35, 483-496.

Masoudian, M. S., Hashemi, M. A., Tasalloti, A., & Marshall, A. M. (2018). Elastic–brittle–plastic behaviour of shale reservoirs and its implications on fracture permeability variation: An analytical approach. Rock Mechanics and Rock Engineering, 1-18.

Mendrinos, D., Karytsas, S., KarytsasC., Poletto, F., Farina, B., (2019), Report on distribution of rock modulus and correlation with temperature, GEMex project deliverable D5.11.

Mendrinos D. et al. (2020), Concept for performance characterisation of the target area, GEMex Deliverable D8.4, in preparation.

Myklestad NO (1942) Two problems of thermal stress in the infinite solid. J Appl Mech 9:136–143

Norini G., Carrasco-Núñez G., Corbo-Camargo F., Lermo J., Rojas J.H., Castro C., Bonini M., Montanari D., Corti G., Moratti G., Piccardi L., Chavez G., Zuluaga M.C., Ramirez M., Cedillo F., (2019). The structural architecture of the Los Humeros volcanic complex and geothermal field, Journal of Volcanology and Geothermal Research, Volume 381, Pages 312-329, ISSN 0377-0273.

Norini G., Groppelli G., Sulpizio R., Carrasco-Núñez G., Dávila-Harris P., Pellicioli C., Zucca F., De Franco R., (2015). Structural analysis and thermal remote sensing of the Los Humeros Volcanic Complex: Implications for volcano structure and geothermal exploration, Journal of Volcanology and Geothermal Research, Volume 301, Pages 221-237, 2015.

Olasolo, P., Juárez, M. C., Morales, M. P., & Liarte, I. A. (2016). Enhanced geothermal systems (EGS): A review. Renewable and Sustainable Energy Reviews, 56, 133-144.

Parisio, F., Vinciguerra, S., Kolditz, O. and Nagel, T., (2019). The brittle-ductile transition in active volcanoes. Scientific reports, 9(1), pp.1-10.

Perkins, T. K., & Gonzalez, J. A. (1984). Changes in earth stresses around a wellbore caused by radially symmetrical pressure and temperature gradients. Society of Petroleum Engineers Journal, 24(02), 129-140.

Perkins, T. K., & Gonzalez, J. A. (1985). The effect of thermoelastic stresses on injection well fracturing. Society of Petroleum Engineers Journal, 25(01), 78-88.

Pijnenburg, R. P. J., Verberne, B. A., Hangx, S. J. T., & Spiers, C. J. (2019). Inelastic deformation of the Slochteren sandstone: Stress-strain relations and implications for induced seismicity in the Groningen gas field. Journal of Geophysical Research: Solid Earth.

Poletto, F., Farina, B., Carcione, J.M., (2018). Sensitivity of seismic properties to temperature variations in a geothermal reservoir. Geothermics 76, 149–163.

Poletto, F., Farina, B., Carcione, J.M., Böhm, G., Mendrinos, D., Jousset, Ph., Pinna, G., Barison, E., (2019a). D5.5: Report on seismic modelling. GEMex Deliverable 5.5.

Poletto, F., Farina, B., Carcione J. M., and Pinna G., (2019b). Analysis of seismic wave propagation in geothermal reservoirs. European Geothermal Congress Den Haag, The Netherlands, 11-14 June 2019.

Rath, V., Wolf, A., Bücker, M., (2006). Joint three-dimensional inversion of coupled groundwater flow and heat transfer based on automatic differentiation: sensitivity, calculation, verification, and synthetic examples, Geophys. J. Int., 167, 453 – 466.

Rice, J. R., & Cleary, M. P. (1976). Some basic stress diffusion solutions for fluid-saturated elastic porous media with compressible constituents. Reviews of Geophysics, 14(2), 227-241.

Rodríguez H., Lermo J., Urban E. (2012), Analysis of Seismic Anisotropy in Los Humeros Geothermal Field, Puebla, Mexico, Proceedings, Thirty-Seventh Workshop on Geothermal Reservoir Engineering, Stanford University, Stanford, California, January 30 - February 1, 2012.

Rutqvist, J., Leung, C., Hoch, A., Wang, Y., & Wang, Z. (2013). Linked multicontinuum and crack tensor approach for modeling of coupled geomechanics, fluid flow and transport in fractured rock. Journal of Rock Mechanics and Geotechnical Engineering, 5(1), 18-31.

Rybach, L., (1976). Radioactive Heat Production: A Physical Property Determined by the Chemistry of Rocks, In: Strens, R. G. J. (ed.), The Physics and Chemistry of Minerals and Rocks, 309 – 318, Wiley & Sons, London

Rybach, L., (1986). Amount and Significance of Radioactive Heat Sources in Sediments, In: Burrus, J. (ed.), Thermal Modelling in Sedimentary Basins, Editions Technip, 311-322.

Schaefer, L.N., Kendrick, J.E., Oommen, T., Lavallée, Y. and Chigna, G., (2015). Geomechanical rock properties of a basaltic volcano. Frontiers in Earth Science, 3, p.29.

Schön, J. H., (2004). Physical Properties of Rocks: Fundamentals and Principles of Petrophysics, 1. Edition, Elsevier, Amsterdam.

Semnani, S. J., White, J. A., & Borja, R. I. (2016). Thermoplasticity and strain localization in transversely isotropic materials based on anisotropic critical state plasticity. International Journal for Numerical and Analytical Methods in Geomechanics, 40(18), 2423-2449.

Settari, A., & Walters, D. A. (2001). Advances in coupled geomechanical and reservoir modeling with applications to reservoir compaction. Spe Journal, 6(03), 334-342.

Shimamoto, T. and Noda, H., (2014). A friction to flow constitutive law and its application to a 2-D modeling of earthquakes. Journal of Geophysical Research: Solid Earth, 119(11), pp.8089-8106.

Singh A., Rao KS, Ayothiraman R. (2019). An analytical solution for a circular wellbore using Mogi-Coulomb failure criterion. Journal of Rock Mechanics and Geotechnical Engineering. (Accepted).

Suter M. (1991), State of stress and active deformation in Mexico and western Central America, The Geology of North America, Decade Map Volume 1.

Tao, Q., & Ghassemi, A. (2010). Poro-thermoelastic borehole stress analysis for determination of the in situ stress and rock strength. Geothermics, 39(3), 250-259.

Tao, J., Wu, Y., Elsworth, D., Li, P., & Hao, Y. (2019). Coupled Thermo-Hydro-Mechanical-Chemical Modeling of Permeability Evolution in a CO2-Circulated Geothermal Reservoir. Geofluids, 2019.

Taron, J., & Elsworth, D. (2009). Thermal–hydrologic–mechanical–chemical processes in the evolution of engineered geothermal reservoirs. International Journal of Rock Mechanics and Mining Sciences, 46(5), 855-864.

Þorbjörnsson, I. Ö. et al (2020). Public summary of the list of material properties and selection guide for Los Humeros North. GEMex Deliverable 8.5.

Verma M.P., Surendra, P. Verma, and Sanvincente H. (1990). Temperature field simulation with stratification model of magma chamber under Los Humeros caldera, Puebla, Mexico. Geothermics, 19 (2), 187-197.

Vinciguerra, S., Trovato, C., Meredith, P. G., & Benson, P. M., (2005). Relating seismic velocities, thermal cracking and permeability in Mt. Etna and Iceland basalts. International Journal of Rock Mechanics and Mining Sciences, 42(7-8 SPEC. ISS).

Violay, M., Gibert, B., Mainprice, D., Evans, B., Dautria, J.M., Azais, P. and Pezard, P., (2012). An experimental study of the brittle-ductile transition of basalt at oceanic crust pressure and temperature conditions. Journal of Geophysical Research: Solid Earth, 117(B3).

Wang, Y., & Dusseault, M. B. (1991, July). Borehole yield and hydraulic fracture initiation in poorly consolidated rock strata—Part II. Permeable media. In International journal of rock mechanics and mining sciences & geomechanics abstracts (Vol. 28, No. 4, pp. 247-260). Pergamon.

Wassing, B. B. T., Van Wees, J. D., & Fokker, P. A. (2014). Coupled continuum modeling of fracture reactivation and induced seismicity during enhanced geothermal operations. Geothermics, 52, 153-164.

Wiesmaier, S., Heap, M.J., Branca, S., Gilg, H.A., Kueppers, U., Hess, K.U., Lavallée, Y. and Dingwell, D.B., (2015). Variability in composition and physical properties of the sedimentary basement of Mt Etna, Italy. Journal of volcanology and geothermal research, 302, pp.102-116.

Wong, T.F. and Baud, P., (2012). The brittle-ductile transition in porous rock: A review. Journal of Structural Geology, 44, pp.25-53.

Zhang, Q., Choo, J., & Borja, R. I. (2019). On the preferential flow patterns induced by transverse isotropy and non-Darcy flow in double porosity media. Computer Methods in Applied Mechanics and Engineering.

Zhao, Y., Semnani, S. J., Yin, Q., & Borja, R. I. (2018). On the strength of transversely isotropic rocks. International Journal for Numerical and Analytical Methods in Geomechanics, 42(16), 1917-1934.

Ziagos, J. P., Blackwell, D. D., Mooser, F. (1985). Heat Flow in Southern Mexico and the Thermal Effects of Subduction. Journal of Geophysical Research, 90, 5410 – 5420.

9 Acknowledgements

We would like to thank the Comisión Federal de Electricidad (CFE) for their support during the GEMex project.

This project has received funding from the European Union's Horizon 2020 research and innovation programme under grant agreement No. 727550 and the Mexican Energy Sustainability Fund CONACYT-SENER, project 2015-04-268074.

Coordination Office, GEMex project

Helmholtz-Zentrum Potsdam
Deutsches GeoForschungsZentrum

Telegrafenberg, 14473 Potsdam

Germany